Budapest University of Technology and Economics
Faculty of Civil Engineering
Department of Hydraulic and Water Resources Engineering

Wave-driven turbulent momentum and heat exchanges at the air-water interface of lakes

Hullámzáskeltette turbulens impulzus- és hőáramok becslése tavi légkör-víz határfelületen

By:
Gabriella Lükő
[*gabriella.luko@gmail.com*]

Advisor:
Péter Torma, associate professor

Budapest, 2019

Contents

Abstract

Turbulent momentum and heat exchanges represent hydrodynamic exchange processes at the air-water interface, and they directly impact ecological conditions, water quality and operational tasks of a lake. Turbulent fluxes can be quantified based on both observational estimation and modeling methods following the oceanographic literature. Momentum and heat fluxes can be calculated locally using the flux-gradient method, which is based on the Monin-Obukhov similarity theory (MOST). Recent studies showed that the available formulas developed after oceanographic observations cannot be used for small-scale and strongly fetch-limited lakes since the developing wave field is mostly characterized by young waves that i) are steeper, and ii) travel with lower phase velocity, than in typical open ocean circumstances. This hypothesis agrees with other modeling experiments of our department. Besides the local exchange of momentum and heat, it is important to explore the spatial variability of them, such as the internal boundary layer development above the water surface. There were very few observation programs for such spatial analysis, and the available models usually use the same MOST formulations.

In this study, a detailed review of the relevant literature is done, then new formulas are developed to estimate the air-water turbulent momentum and heat exchanges for shallow lakes using observation data series. In present study the data of the monitoring stations in the bay of Keszthely in Lake Balaton have been used, which consisted of high frequency meteorological measurements together with acoustic surface tracking and current profiler instruments. Not only the wind speed, air temperature and humidity data are used, but the effect of the waves are taken into account for the estimation of different exchanges as well. Thanks to the three simultaneously operating stations, which were installed along the fetch of the prevailing wind direction, the effect of the spatial variability can be analyzed. With the resulted, new formulas precise boundary conditions can be provided for a hydrodynamic model, which could serve as a base of a lake forecasting system if the model is detailed enough both in the description of the physical processes and in spatial resolution as well.

Kivonat

A légkör-víz határfelületen kialakuló hidrodinamikai cserefolyamatok impulzus- és hőáramok formájában jelentkeznek, amelyek közvetlenül alakítják a tó ökológiai állapotát és vízminőségét. Ezen folyamatok számszerű leírására számos oceanográfiai kutatás irányul, amelyek különféle mérési és becslési módszereken, valamint modelleken alapulnak. A turbulens impulzus- és hőáramok profil alapú, fluxus-gradiens eljárással számíthatók lokálisan, amely a Monin-Obukhov-féle hasonlósági elméleten (MOST) alapszik. Friss kutatások azt mutatják, hogy az oceanográfiai mérések alapján levezetett összefüggések nem helytállók kisebb léptékű és erősen meghajtási hossz limitált környezetben, ahol a kialakuló hullámok jellemzően fiatalabbak, így i) nagyobb meredekségűek, valamint ii) a fázissebességük is kisebb, mint az óceáni nyílt vízi környezetben. Ezen felvetések összhangban állnak az elmúlt évek tanszéki modellvizsgálatainak eredményeivel. A lokális impulzusátadás és hőcsere mellett természetesen fontos azok térbeli változékonyságának ismerete, mint például a vízfelszín felett fejlődő belső légköri határréteg fejlődése. Ilyen térbeli vizsgálatra kevés mérési program irányult idáig, míg az ennek leírására irányuló modellek sok esetben szintén a MOST összefüggéseit használják.

Dolgozatomban részletes irodalomkutatást követően terepi mérések adatsorai alapján kísérletet teszek új, sekély tavi, meghajtási hossz limitált körülményekre alkalmazható légkör-víz határfelületen kialakuló impulzusáram becslő összefüggések levezetésére. Jelen kutatás alapját a Balaton Keszthelyi-öblében telepített nagyfrekvenciájú nyomás-, áramlás- és vízszintmérővel kiegészített meteorológiai mérőállomások adatsorai képezik. Nemcsak a légköri oldal szélsebesség, hőmérséklet és nedvességtartalom adatait használom fel, hanem a hullámzás hatását is figyelembe veszem. A három egyszerre működtetett és szélmeghajtási irány mentén elhelyezett mérőállomásnak köszönhetően a térbeli változékonyságot is vizsgálni fogom. Az eredményként kapott összefüggésekkel lehetőségünk lesz a sekély tavakra alkalmazott hidrodinamikai modellek számára pontos peremfeltételek biztosítására, amelyek, ha kellően részletesek a fizikai folyamatok leírásában és térbeli felbontásukban is, egy előrejelző-rendszer alapjául szolgálhatnak.

1   Introduction

Turbulent momentum and heat fluxes represent hydrodynamic exchange processes at the air-water interface, and they directly impact ecological conditions and water quality through water temperature and mixing. In this study turbulent fluxes are quantified based on observational estimations; however, the literature dominantly arises from oceanography. The motivation of this study was to estimate primarily the momentum flux, and secondarily heat fluxes of Lake Balaton mainly for hydrodynamic modeling purposes. The main feature of Lake Balaton that generates deviation compared to typical oceanographic conditions, is the short fetch. Coastal studies of oceans already use other parameterization for fetch-limited environment, but the analyzed lake is even more different. The wave age is a dimensionless parameter used for the flux estimations, so the characteristics of the wave field can be considered as well. The wave field of Lake Balaton has very young and high frequency waves, while the typical significant wave height is about 20-50 cm. Fig. 1.1 shows that the measured inverse wave age values are far above the literature data that was collected by Edson et al. (2013) from several sources to improve the commonly used COARE algorithm (Fairall et al. 2003).
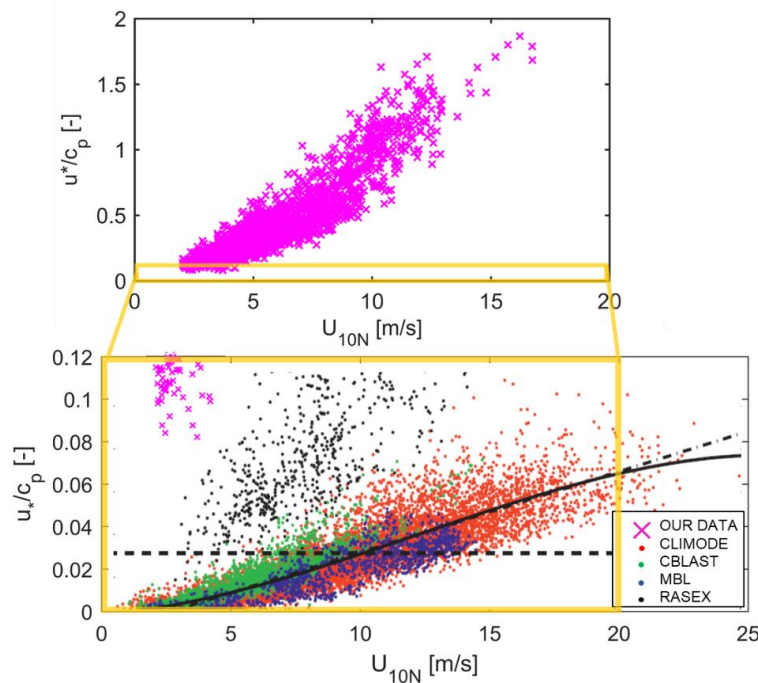

Fig. 1.1 Inverse wave age as a function of wind speed for our data and data collection made by Edson et al. (2013)

Consequently, the currently available drag and heat transfer coefficients and exchange parameterizations in the oceanographic literature are not applicable to estimate the turbulent fluxes in Lake Balaton and in highly fetch-limited conditions in general. The hypothesis is that the resistance of the airflow over these young and steep waves is significantly higher than in typical oceanographic environment.

2 Theoretical background

The turbulent motions (x), such as momentum and heat fluxes in the atmosphere, or in general can be decomposed as:

$$x = \bar{x} + x'$$

where $\bar{x}$ is the mean of the variable and x' is the turbulent fluctuation component. It is accepted that the vertical gradients of wind speed, temperature and humidity covariances are nearly zero, and it means the covariances are constant with height in the surface layer:

$$\frac{\partial \overline{u'w'}}{\partial z} \approx 0$$

$$\frac{\partial \overline{T'w'}}{\partial z} \approx 0$$

$$\frac{\partial \overline{q'w'}}{\partial z} \approx 0$$

where the u is horizontal, w is vertical wind component, T is the air temperature and q is the specific humidity of air from high frequency measurements. The covariance of the vertical wind velocity, w, and a horizontal wind component or a scalar, x, can be determined by:

$$\overline{w'x'} = \frac{1}{N-1} \sum_{k=0}^{N-1} [(w_k - \overline{w_k})(x_k - \overline{x_k})] =$$
$$= \frac{1}{N-1} \left[\sum_{k=0}^{N-1} w_k x_k - \frac{1}{N} \left(\sum_{k=0}^{N-1} w_k \sum_{k=0}^{N-1} x_k \right) \right]$$

This means that the total flux is equal to the covariance. The implementation of this equation is the eddy-covariance measuring technique, where the turbulent fluxes can be determined directly:

$$u_*^2 = -\overline{u'w'}$$

$$\frac{HTs}{\rho_a \cdot c_{pH}} = \overline{T'w'}$$

$$\frac{L_v E}{\rho_a \cdot \lambda} = \overline{q'w'} \qquad \text{Eq. 2.8}$$

where u_* is the friction velocity, HTs is the sensible and L_vE is the latent heat fluxes, ρ_a is the air density, c_{pH} is the specific humidity of air at constant pressure and λ is the latent heat of vaporization. The momentum flux or surface stress (τ) is the drag per unit area of water surface, but it is often expressed with only the friction velocity (u_*). The momentum flux is usually parametrized with the drag coefficient (C_D). Similar for the sensible and latent heat fluxes, which are parametrized with the heat transfer coefficients (C_H and C_q). These bulk parametrization equations are as follows:

$$u_*^2 = C_{Dz} \cdot U_z^2 = \frac{\tau}{\rho_a} \qquad \text{Eq. 2.9}$$

$$HTs = \rho_a \cdot c_{pH} \cdot C_{Hz} \cdot U_z \cdot (T_z - T_0) \qquad \text{Eq. 2.10}$$

$$L_v E = \rho_a \cdot \lambda \cdot C_{qz} \cdot U_z \cdot (q_z - q_0) \qquad \text{Eq. 2.11}$$

where U_z is the averaged wind speed, T_0 is the water surface temperature of, q_0 is the specific humidity of water surface. Usually, potential temperature of air (θ_z) and water surface (θ_0) are used instead of simple temperature values. Following the Monin-Obukhov similarity theory (MOST) (Monin and Obukhov 1954) the drag coefficient, sensible and latent heat transfer coefficients can be calculated as:

$$C_{Dz} = \left(\frac{\kappa}{\ln\left(\frac{z}{z_0}\right) - \psi_m\left(\frac{z}{L}\right)} \right)^2 \qquad \text{Eq. 2.12}$$

$$C_{Hz} = \left(\frac{\kappa}{\ln\left(\frac{z}{z_0}\right) - \psi_m\left(\frac{z}{L}\right)} \right)\left(\frac{\kappa}{\ln\left(\frac{z}{z_{0H}}\right) - \psi_H\left(\frac{z}{L}\right)} \right) \qquad \text{Eq. 2.13}$$

$$C_{qz} = \left(\frac{\kappa}{\ln\left(\frac{z}{z_0}\right) - \psi_m\left(\frac{z}{L}\right)} \right)\left(\frac{\kappa}{\ln\left(\frac{z}{z_{0q}}\right) - \psi_q\left(\frac{z}{L}\right)} \right) \qquad \text{Eq. 2.14}$$

where κ is the von Kármán constant, z_0 is the roughness length for momentum, z_{0H} roughness length for temperature and z_{0q} roughness length for humidity, ψ_m, ψ_H, and ψ_q are stability functions of for different stability conditions and L, is the so-called Obukhov length:

$$L = \frac{u_*^2 T}{\kappa g (T_* + 0.61 T q_*)} \qquad \text{Eq. 2.15}$$

where T_* is the temperature scale, q_* is the scale of mixing ratio from the covariance measurements and g is the acceleration of gravity. According to the MOST wind speed, temperature and specific humidity profiles above the surface are logarithmic:

$$U_z = \frac{u_*}{\kappa}\left(\ln\left(\frac{z}{z_0}\right) - \psi_m\left(\frac{z}{L}\right)\right)$$

Eq. 2.16

$$T_z - T_0 = \frac{T_*}{\kappa}\left(\ln\left(\frac{z}{z_{0H}}\right) - \psi_H\left(\frac{z}{L}\right)\right)$$

Eq. 2.17

$$q_z - q_0 = \frac{q_*}{\kappa}\left(\ln\left(\frac{z}{z_{0q}}\right) - \psi_q\left(\frac{z}{L}\right)\right)$$

Eq. 2.18

The roughness lengths of momentum, heat and humidity are usually calculated from the stability corrected logarithmic profiles unless atmospheric stratification is near neutral ($z/L \sim 0$). In order to do that, the stability functions need to be chosen. There are several empirical functions available to use or they can also be derived from the available measured stratification parameters, such as z/L, These are the most commonly used stability functions (Dyer 1974):

- for instable conditions ($z/L < 0$):

$$\psi_m = 2\cdot\ln\left(\frac{1 + {\Phi_m}^{-1}}{2}\right) + \ln\left(\frac{1 + {\Phi_m}^{-2}}{2}\right) - 2\cdot tan^{-1}\cdot\left({\Phi_m}^{-1}\right) + \frac{\pi}{2}$$

Eq. 2.19

$$\psi_h = \psi_q = 2\cdot\ln\left(\frac{1 + \left(\left(1 - 8\left(\frac{z}{L}\right)\right)^{0.25}\right)^2}{2}\right)$$

Eq. 2.20

where Φ_m can be originally calculated if there are measurements available at multiple heights:

$$\Phi_m = \frac{\kappa z}{u^*}\cdot\frac{\partial U}{\partial z}$$

Eq. 2.21

but it can be well estimated as a function of z/L:

$$\Phi_m = \left(1 - \alpha_m\cdot\left(\frac{z}{L}\right)\right)^{-1/4}$$

Eq. 2.22

where α_m is determined in literature: $\alpha_m = 16$ (Lin et al. 2002), $\alpha_m = 20$ (Shabani et al. 2014).

- for stable conditions ($z/L > 0$):

$$\psi_m = -\beta_m \cdot \left(\frac{z}{L}\right)$$

<div align="right">Eq. 2.23</div>

$$\psi_h = \psi_q = \gamma \left(1 - 7.8 \left(\frac{z}{L}\right)\right)$$

<div align="right">Eq. 2.24</div>

where $\beta_m = 5$ (Shabani et al. 2014), $\beta_m = 7$ (Lin et al. 2002) and $\gamma_h = 0.74$, $\gamma_q = 1$ both from Brutsaert (1982). Now, the roughness lengths can be finally calculated for all stability conditions if momentum (u_*), temperature (T_*) and humidity (q_*) scales are known:

$$z_0 = \frac{z}{e^{\left(\frac{\kappa}{u_*} \cdot U_z + \psi_m\left(\frac{z}{L}\right)\right)}}$$

<div align="right">Eq. 2.25</div>

$$z_{0H} = \frac{z}{e^{\left(\frac{\kappa}{T_*}(T_z - T_0) + \psi_H\left(\frac{z}{L}\right)\right)}}$$

<div align="right">Eq. 2.26</div>

$$z_{0q} = \frac{z}{e^{\left(\frac{\kappa}{q_*}(q_z - q_0) + \psi_q\left(\frac{z}{L}\right)\right)}}$$

<div align="right">Eq. 2.27</div>

The roughness length calculation is essential unless there are wind measurements at multiple heights to define the 10-meter neutral wind speed:

$$U_{10N} = \frac{u^*}{\kappa} \cdot \ln\left(\frac{10}{z_0}\right)$$

<div align="right">Eq. 2.28</div>

The 10-meter neutral drag and heat transfer coefficients can be calculated as well:

$$C_{D10N} = \left(\frac{u_*}{U_{10N}}\right)^2 = \left(\frac{\kappa}{\ln\left(\frac{10}{z_0}\right)}\right)^2$$

<div align="right">Eq. 2.29</div>

$$C_{H10N} = \left(\frac{\kappa}{\ln\left(\frac{10}{z_0}\right)}\right)\left(\frac{\kappa}{\ln\left(\frac{10}{z_{0H}}\right)}\right)$$

<div align="right">Eq. 2.30</div>

$$C_{q10N} = \left(\frac{\kappa}{\ln\left(\frac{10}{z_0}\right)}\right)\left(\frac{\kappa}{\ln\left(\frac{10}{z_{0q}}\right)}\right)$$

<div align="right">Eq. 2.31</div>

The corrected U_{10N} and C_{D10N}, C_{H10N}, C_{E10N} values now can be analyzed equally and they are not affected by the applied different measurement heights nor the stratification given differences either. This is also the unified method in the literature, so the momentum and heat exchange estimations can be easily applied and compared to others. Besides the drag coefficient, there is another widely used momentum flux estimation parameter developed by Charnock (1955):

$$z_0 = \alpha \cdot \frac{u^{*2}}{g} + 0.11 \cdot \frac{\nu}{u^*}$$

Eq. 2.32

where ν is the kinematic viscosity and α is the Charnock constant. Charnock alpha was originally estimated as a constant, but there are modified Charnock formulations as well. These modified formulas consider the effect of the wave field. Besides the significant wave height, the wave field is usually characterized by non-dimensional parameters as such the wave age and wave steepness. The wave age is defined as:

$$\frac{c_p}{u_*}$$

Eq. 2.33

where c_p is the wave phase velocity and u_* is the same friction velocity from the atmosphere. The wave age is often expressed with its inverse value (u_*/c_p) and sometimes with the wind speed in the denominator (c_p/U_{10}) or its inverse (U_{10}/c_p). The wave steepness is defined as:

$$\frac{H_s}{L}$$

Eq. 2.34

where H_s is the significant wave height and L is the wavelength.

3   Literature review

According to the exclusive literature research, it can be stated that most of studies are from meteorology and oceanography and only a few have been done by limnology groups. The studies primarily concentrate on the momentum flux of the air-water interface and apply the bulk parameterization and MOST-based estimations. The data ranges and derived equations from the literature are summarized in Table 3.1. Smith et al. (1992) had both offshore open ocean and onshore measurements at the North Sea, and the campaigns were called HEXOS, HEXMAX and MPN (with the short 5 km fetch). They set up the Charnock alpha - wave age relationship but it is affected with self-correlation; different c_D-U_{10} functions for young, mature and fully developed waves; $z_0/H_s = f(U_{10}/c_p)$, which avoids self-correlation, but the sea state was dominated by swell. Taylor and Yelland (2001) used published data (HEXMAX, RASEX, Lake Ontario) and done roughness length prediction from $z_0/H_s = f(H_s/L)$. There were fractional changes in drag coefficient as a function of duration, depth and fetch at different wind speeds. The formula could not predict the high C_D values observed over Lake Ontario, because the very young waves are rare in datasets, which is not the case in our measured Lake Balaton data. Vickers and Mahrt (1997) had offshore and onshore measurements at the Baltic Sea in Denmark called RASEX with short fetch of 2 - 5 km in shallow water. They calculated Charnock constant and it is $\alpha = 0.073$ offshore and $\alpha = 0.018$ onshore. They measured large drag coefficients as well. They separated seven wave age categories when showed drag coefficients as a function of wind speed. They derived modified Charnock formulation, such as drag coefficient as a function of wave age and other wave parameters, based on frequency bandwidth of wave spectrum. Johnson et al. (1998) used new combined RASEX data, but with 15 - 20 km fetch. They derived the modified Charnock alpha as a function wave age, and it was compared with other compiled datasets as well. Lin et al. (2002) had simultaneous air-sea flux, wave and surface current data from Chesapeake Bay in the east coast of US with fetch limited and low winds conditions. The drag coefficient depends on both wind speed and wave age, but better correlated to wave age and they have lower drag coefficients than in other datasets. They also used numerical wave model to predict wave age dependent drag coefficients. Oost et al. (2002) had data from the North Sea with 9 km fetch, and lower measured wave age values. They had linear u_*/g - H_s/c_p relationship with no self- correlation; and linear inverse wave age - steepness relationship and found exponential Charnock alpha - wave steepness relationship, and exponential Charnock alpha – wave age relationship, but again with self-correlation. Drennan et al. (2003) used five field campaigns (two datasets from Lake Ontario, one of each from the coast of Virginia, the North Sea, and the Gulf of Lion) together to do a more complete analysis on turbulent momentum exchange. They used Charnock parametrization as a function of inverse wave age and roughness length - inverse wave age relation, because the last one avoids self-correlation in the friction velocity. They said that the wave age dependence is a significant factor, which is very important in our case, since our data has young waves, while typical oceanographic circumstances are characterized by grown and fully developed waves. Babanin and

Makin (2008) have done drag coefficient parametrization taking into account the effects of wind trend and gustiness using experimental data series from Lake George in Australia. Note that this is the first study from a shallow lake. The air-sea interaction is analyzed with the Wind-Over-Waves Coupling (WOWC) model. They also analyzed the drag dependence on the sea-state with Charnock-type wave age relation. Kumar et al. (2009) had data from the Indian Ocean and applied different C_D - U_{10} plots for several wave age intervals, but mainly the young $c_p/u_* < 15$ and growing $c_p/u_* = 15$ - 20 can be interesting for comparison with our data. Shabani et al. (2014) had data from the East Australian coast and applied different stability groups for C_D - U_{10} plots. Their onshore data points are completely off the twelve literature equations for C_D - U_{10} and C_D - c_p/u_* plots as well, because the C_D values are twice as high as in other studies. Fisher et al. (2015) used observation data collection from Chesapeake Bay of wind stress and used SWAN numerical modeling for waves. They found high variability of Charnock alpha between open ocean values and strongly fetch limited values and established $C_D = f(U_{10})$, $C_D = f(c_p/u_*)$ and $\alpha = f(c_p/u_*)$ relations.

There are some novel studies that question MOST and attempt to develop simpler formulations. Andreas et al. (2012) worked with large near-surface eddy-covariance dataset and set up a linear relation between the friction velocity and the 10-m neutral wind speed for the air-sea drag estimation. They said that its advantages that U_{10} have smaller experimental uncertainty than C_D calculations; in scatterplots C_D is ill posed when U_{10} is small; and this method weakly depends on the MOST. Vickers et al. (2015) had aircraft eddy-covariance measurements from nine different experiments and developed a simple model for friction velocity. It does not use the MOST at all and does not need to estimate the Obukhov length; does not need wind speed correction for height and stability and so does not need to estimate roughness length either, which have large uncertainty; and the method does not use iteration. This simple model is basically a third-order polynomial of the friction velocity as a function of wind speed from different heights, but for the near neutral cases only.

There are significantly less studies where heat fluxes are also analyzed next to the momentum. Xiao et al. (2013) had eddy-covariance data at three sites from a shallow lake, Lake Taihu in China. Transfer coefficients were analyzed, and the results indicate that they decreased with increasing wind speed for weak winds and approached constant values for strong winds. The presence of submerged macrophytes reduced the drag coefficient significantly. Wang et al. (2015) had data from Lake Nam Co, one of the lakes in Tibetan Plateau. The lake-air heat and water vapor turbulent transfer processes were evaluated with two popular lake-air exchange models: a bulk aerodynamic transfer and a multilayer model. Observations show that the bulk transfer coefficient (C_q) and roughness length (z_{0q}) for water are higher than those for heat (C_H and z_{0H}), especially under low wind speed; both models underestimate turbulent fluxes due to inaccurate values of the Charnock coefficient (α) which is important parameters for calculating the roughness length for momentum (z_0) over water; α is within a reasonable range of $0.013 - 0.035$ for rough flow. The wave pattern of shorter wavelength gives a larger z_0 in the small and

shallow lake. Li et al. (2016) had EC data from the Ross Barnett Reservoir in Mississippi and it was analyzed to study how atmospheric stability and other variables modulated L_vE and HTs variations in different stability ranges. The results demonstrated that the maximum (minimum) L_vE and HTs did not necessarily occur under the most unstable (stable) conditions, but rather in the intermediate stability ranges. No individual variables were able to explain the dependence of L_vE and HTs variations on stability, but the coupled variables of wind speed, vapor pressure gradient, and temperature gradient. Yusup and Liu (2016) collected eddy covariance flux data from Lake Ngoring in China to analyze the variation of transfer coefficients and roughness lengths for momentum, heat and moisture and compare the results in a lake model. The drag coefficient rapidly decreased with increasing wind velocity, reached a minimum value in the moderate wind velocity and then increased slowly as wind velocity increased further. The lake model could not reproduce well the variation of drag coefficient, or momentum roughness length, versus wind velocity in Lake Ngoring, but it did simulate well the sensible heat and latent heat fluxes. Wang et al. (2017) used long-term evaporation and energy budget observation data from a small lake in the Nam Co basin. The bulk aerodynamic transfer model provides reliable and consistent results. The wind speed shows significance at half hourly scale, but water vapor and temperature gradients have higher correlations over daily and monthly scales in lake-air turbulent heat exchange.

Table 3.1 Data ranges and derived equations in the literature for momentum flux

	Wind		Wave bulk parameters			Wave age				$C_D \cdot 10^{-3}$ [-]	Drag coefficient		Charnock α	Wave steepness
	U_{10} [m/s]	u^* [m/s]	H_s [m]	f_p [Hz]	Fetch [km]	c_p/u^* [-]	u^*/c_p [-]	c_p/U_{10} [-]	U_{10}/c_p [-]		$C_D \cdot 10^{-3}$ eq.	C_D eq.	α eq.	H_s/L [-]
Smith et al. 1992	0-10	-	-	-	5	10-30	0.03 - 0.1	-	-	1 - 3	$0.036 \cdot U_{10} + 1.11$	-	$0.48 \cdot (c_p/u^*)^{-1.0}$	-
Vickers & Mahrt 1997	1-17	-	0.2 - 1.4	0.15 - 0.25	2-5	8-40	0.03 - 0.13	0.3-1.5	0.67 - 3.3	0.5 - 2.2	$0.067 \cdot U_{10} + 0.75$	$0.0071 \cdot (c_p/u^*)^{-0.67}$	$2.9 \cdot (c_p/u^*)^{-2.0}$	0.02 - 0.05
Johnson et al. 1998	4-17	0.16 - 0.7	0.18 - 0.71	0.26 - 0.48	10-20	5-50	0.02 - 0.2	-	-	1.2 - 2	-	-	$1.9 \cdot (c_p/u^*)^{-1.6}$	-
Taylor & Yelland 2001	10-20	-	2-4	-	7	10-30	0.03 - 0.1	0.5-1.1	1-5	1.3 - 3.3	$0.87 + 0.075 \cdot U_{10} - 0.000661 \cdot U_{10}^2$	-	-	0.005 - 0.05
Lin et al. 2002	1-10	-	0.1 - 0.6	0.25 - 0.5	3-10	10-80	0.013 - 0.1	-	-	0.5 - 3	$0.065 \cdot U_{10} + 0.70$	$0.0068 \cdot (c_p/u^*)^{-0.59}$	-	-
Oost et al. 2002	2-12	0.05 - 0.5	-	-	9	0-12	0 - 0.08	0.7-1.5	0.67 - 1.42	0.5 - 3	$0.14 \cdot U_{10} + 0.18$	-	$\ln(\alpha) = -2.5 \cdot \ln(c_p/u^*) + 3.9$ $\ln(\alpha) = 2.2 \cdot \ln(H_s/L) + 3.2$	0 - 0.08
Drennan 2003	5-20	0.2 - 0.8	0.5 - 3	0.1 - 0.4	0-20	10-30	0.03 - 0.1	-	-	0.5 - 2	-	-	$1.7 \cdot (c_p/u^*)^{1.7}$	-
Babanin & Makin 2008	4-23	0.13 - 0.98	0.08 - 0.46	0.33 - 1.14	-	6-13	0.08 - 0.15	0.17 - 0.5	2-6	0.91 - 3.1	$1.9 \cdot 10^{-4} \cdot U_{10}^3 + 0.96$	$9.3 \cdot 10^{-7} \cdot (U_{10}/c_p)^4 + 0.00096$	-	0.06 - 0.2
Kumar et al. 2009	2-22	-	-	-	-	10-	-	-	-	0.5 - 4	$0.41 + 0.13 \cdot U_{10} + 10^{-3} \cdot 1.1 * U_{10}^2$ (for $c_p/u^* < 15$)	-	-	-
Shabani et al. 2014	3-13	0.37	1-3	0.08 - 0.2	10	25-50	0.02 - 0.04	-	-	1-2	-	-	-	-
Fisher et al. 2015	5-16	0.15 - 0.7	0.1 - 1.2	0.2 - 0.8	9	5-20	0.05 - 0.2	-	-	0.8 - 2.1	$0.075 \cdot U_{10} + 0.67$	$0.0041 \cdot (c_p/u^*)^{-0.43}$	$0.14 \cdot (u^*/c_p)^{0.93}$	-

4   Measurements

4.1   Location

In order to prove our hypothesis, high quality data have been collected from several locations in Lake Balaton in 2018 and 2019 (Fig. 4.1). The lake is very shallow and, having an average depth of $d = 3.2$ m and the surface area of $A = 600$ km^2. To gain a detailed insight into spatial variations, three measurement stations were set up along the fetch of the prevailing wind direction, in the bay of Keszthely in the framework of the FIMO-CROHUN (FIrst MicrOmeteorological research within CROatian-HUNgarian collaboration) project in 2018 and the stations operated for about one and a half month.
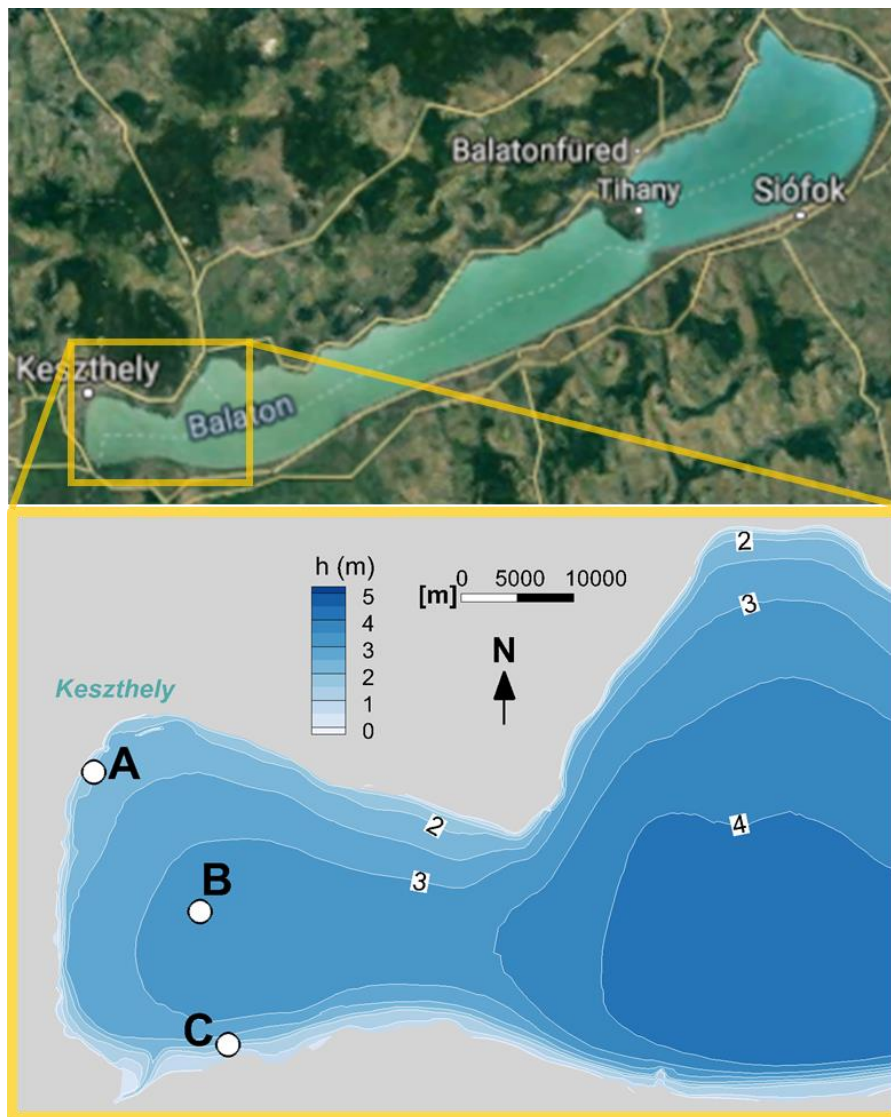
Fig. 4.1 Measurement location in Lake Balaton

The three stations (Fig. 4.2) with the fetch for prevailing wind direction:

- Station A at Keszthely near the shore (fetch ~ 0.1 km, depth ~ 1.4 m),
- Station B in the middle of the bay (fetch ~ 3.5 km, depth ~ 3.4 m), and
- Station C at the south shore (fetch ~ 6 km, depth ~ 1.5 m).

This measurement set up makes possible both the spatial and temporal analysis of turbulent exchanges at the air-water interface, such as we can explore the internal boundary layer (IBL) development (Torma 2016).

Fig. 4.2 Station A, B and C (respectively) in 2018

After the successful campaign in 2018, the offshore station B was set up again in 2019 in the middle of the bay very close to the 2018 location. It operated almost for five months from May until October 2019 and the set up can be seen in Fig. 4.3.

Fig. 4.3 Station B in 2019

4.2   Instrumentation

4.2.1 Campaign 2018 (FIMO-CROHUN)

Turbulent heat and momentum fluxes were measured by an eddy-covariance (EC) set-up which consisted of a 3D sonic anemometer and an open path gas analyzer at the offshore station. At the onshore stations sonic anemometers provided momentum and sensible fluxes. The wave field was measured at the offshore station. The air temperature and humidity data and the water surface temperature data were used for the bulk estimation. All meteorological instruments measured between 31st August – 11th October 2018. The wave and current profiles were measured between 13th September – 11th October 2018. So, the three stations had this selection of instruments, from which I highlight those with bold fonts which are used in the present study:

Station A (Onshore):

- 3D sonic anemometer (Campbell CSAT3) – 10 Hz
- Air temperature & humidity sensor (Vaisala HMP45)
- Thermistors 4+1 (Campbell T107)

Station B (Offshore):

Air side:

- **Eddy-covariance (EC) (CSAT3 + EC150) – 10 Hz**
  Campbell Scientific's CSAT3 is the 3D sonic anemometer for eddy-covariance measurements. Campbell Scientific's EC150 is an open-path analyzer specifically designed for eddy-covariance carbon and water flux measurements. The two together measure three-dimensional wind speed, sonic air temperature and moisture.
- Net radiometer (CNR4)
- **Air temperature & humidity sensor (Vaisala HMP45)**
- 2D sonic anemometer (Campbell Windsonic)

Water side:

- **Thermistors 5+3 (Campbell 107)**
- Heat flux plate (Hukseflux)
- PAR sensor
- **Wave (Nortek Signature1000) – 4 Hz**
  The Signature1000 ADCP is the optimal tool for turbulence measurements with a maximum sampling frequency of 16 Hz. High vertical resolution current profiles and it can measure wave height and direction.
- Current profiler (Nortek Aquadopp)

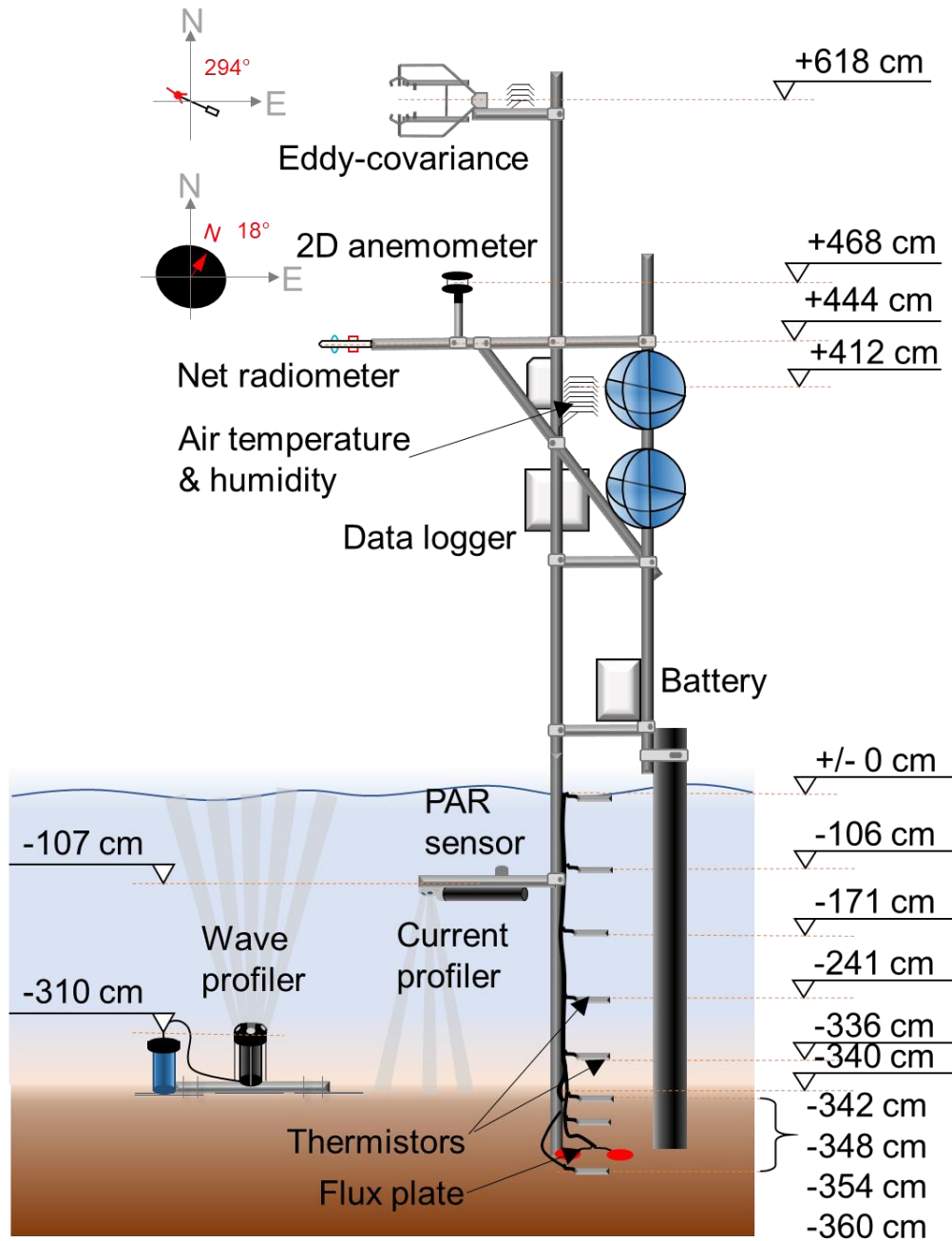The schematic drawing of the offshore station B in 2018 can be seen in Fig. 4.4.

Fig. 4.4 Instrumentation of the offshore station B in 2018

Station C (Onshore):

- 3D sonic anemometer (Gill Windmaster) – 10 Hz
- Air temperature & humidity sensor (HMP45)
- Thermistors 4+1 (Campbell T107)

It is noted, that the onshore station C with the longest fetch was destroyed by a heavy storm at 26 September 2018, so data is available only for a three-week-long period.

4.2.2 Campaign 2019

In 2019 the offshore station operated between 18th May – 8th October 2019. On the water side, the wave and current measurements operated since 11th June 2019 until October. The instrumentation is similar like in 2018:

Station B (Offshore):

Air side:

- Eddy-covariance (EC) (CSAT3+EC150) – 10 Hz
- Net radiometer (CNR4)
- Air temperature & humidity sensor (Vaisala HMP45)
- 2D anemometer (Campbell Windsonic)

Water side:

- Thermistors 6+3 (Campbell T107)
- Heat flux plate (Hukseflux)
- PAR sensor
- Wave profiler (Nortek Signature) – 4 Hz
- Current profiler (Nortek Aquadopp) – 4 Hz
- Current meter (Nortek Vector) – 8 Hz

The instrumentation of station B in 2019 can be seen in Fig. 4.5. Next to the new and more practical arrangement of the instruments, the only difference there is compared to the station in 2018, that the flow measurements were completed with a Nortek Vector current meter operating at 8 Hz below the water surface.
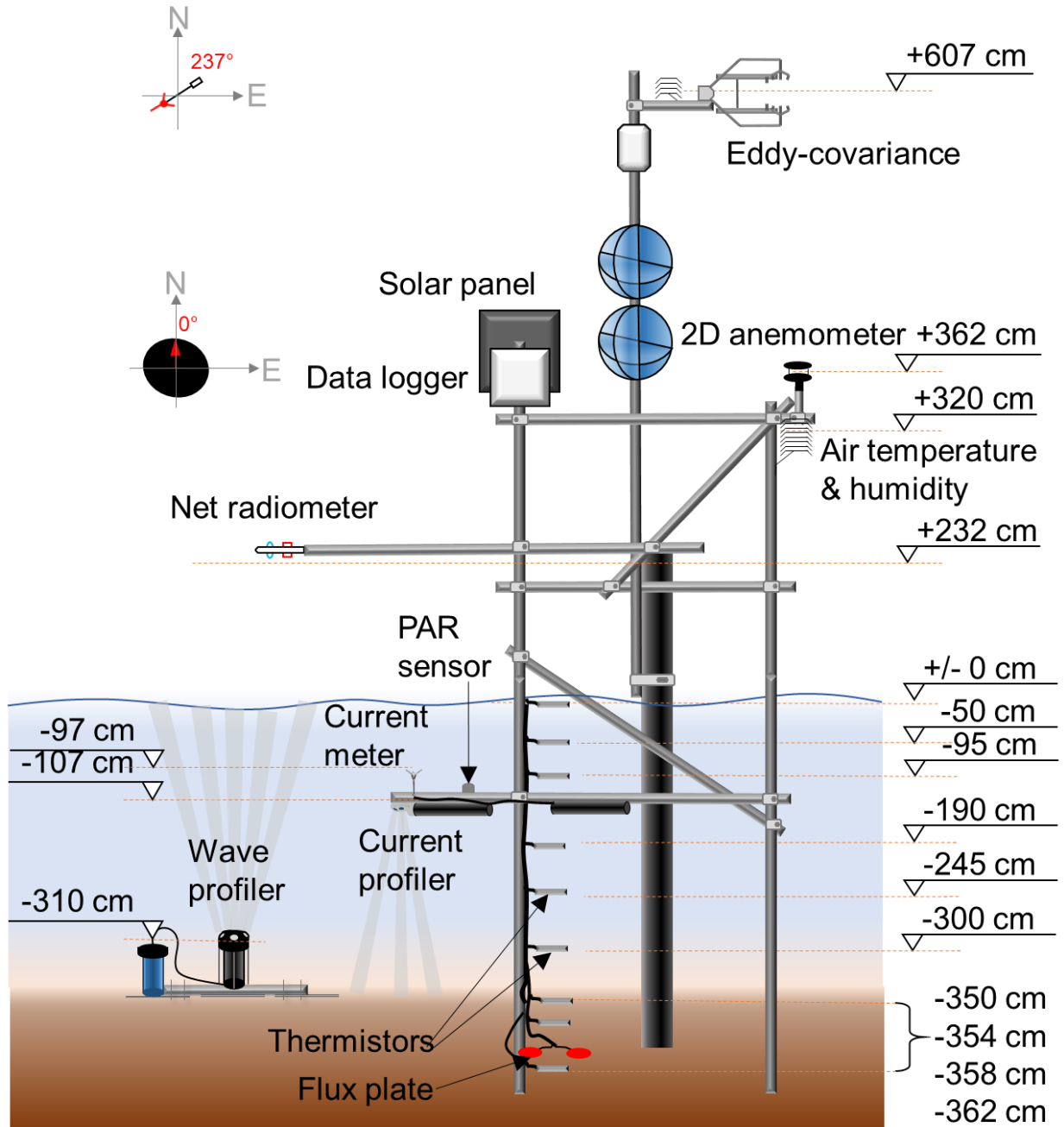
Fig. 4.5 Instrumentation of the offshore station B in 2019

5   Methods

5.1   EC data processing & calculation

The eddy-covariance technique measures the fluctuational components of wind, temperature and moisture at high frequency and accurately synchronized manner. From which first the covariances (Eq. 2.5) and the turbulent fluxes of momentum (Eq. 2.6) and heat fluxes (Eq. 2.7 Eq. 2.8) can be calculated.

The raw flux data from the CSAT3+EC150 eddy-covariance (EC) instruments were first converted to ASCII files. Then it was post-processed with the Turbulent Knight 3 (TK3) software developed at Bayreuth University (Mauder and Foken 2011) which consisted of 20-min-average calculation (e.g. HH:20-HH:40); spike filtering with no filling up of missing values; double rotation and rotation into mean wind direction (Wilczak et al. 2001); Moore correction of spectral loss; Schotanus correction from buoyancy flux; WPL correction of density fluctuation (Webb and Leuning 1980).

Both datasets from 2018 and 2019 had ~2-week-long raw data series. First, they have been post-processed with TK3 and then the timeseries were imported and merged using own MATLAB scripts. So, the final data table is available for 31 August – 11 October 2018 & 18 May – 4 September 2019 together. The rest of the data until October 2019 have not been processed yet. This time series will be referred to as raw data later.

The measured atmospheric data were the following:

U_z	[m/s]	wind speed at z height
dir	[°]	wind direction (0° - North)
z	[m]	measurement height from water surface
u_*	[m/s]	momentum flux
z/L	[-]	stability condition
σ_w/u_*	[-]	turbulence characteristic
T_w	[°C]	water surface temperature (from the thermistor data)
T_a	[°C]	air temperature at z height
RH	[%]	relative humidity of air
p	[Pa]	air pressure
HT_s	[W/m^2]	sensible heat flux
$L_v E$	[W/m^2]	latent heat flux

The raw EC data have been filtered with the following quality assurance (QA) and quality control (QC) filters (Foken 2008). These filters have been applied and tested, also in MATLAB: the vertical average wind speed component must be zero ($\overline{w'} = 0$); with 1-9 quality classes after Foken et al. (2004), where data accepted if QC < 7.

The flux variance test or integral turbulence characteristics test, where data accepted if there is a maximum of +/- 40 % difference between measured and theoretical values, and it is applied separately for different stability conditions:

- neutral: $\frac{\sigma_w}{u_*} = c$

- stable: $\frac{\sigma_w}{u_*} = c\left(\frac{z}{L}\right)$

- unstable: $\frac{\sigma_w}{u_*} = 1.25\left(1 - 2\frac{z}{L}\right)^{1/3}$

Minimum limiters have been also applied as filters because of stationarity, like $\Delta U_{10N} < 50\ \%$ and $\Delta dir < 30\ °$, so it cannot be too fast changes in wind speed and wind direction values between two consecutive 20-min average values. Other minimum limiters have been also applied for very low winds, like $U_{10N} > 2$ m/s and $u_* > 5$ cm/s where free-convection and buoyancy forces dominate (Abdella and D'Alessio 2005).

After the post-processing and QA and QC filtration the flux analysis and calculations can be started to develop estimation methods. The schematic figure of the further momentum flux calculations can be seen in Fig. 5.1, and the heat fluxes have been calculated using similar methodology. All calculations and curve fittings have been done using MATLAB.

First the stability functions were chosen. Then from the stability corrected velocity profile the roughness length of momentum, heat and humidity were calculated. This way the wind speed was corrected to the 10-meter neutral values and the 10-meter neutral drag and heat transfer coefficients and Charnock-alpha vales were calculated as well. After that, several different momentum and heat flux estimation methods have been applied and tested from those.
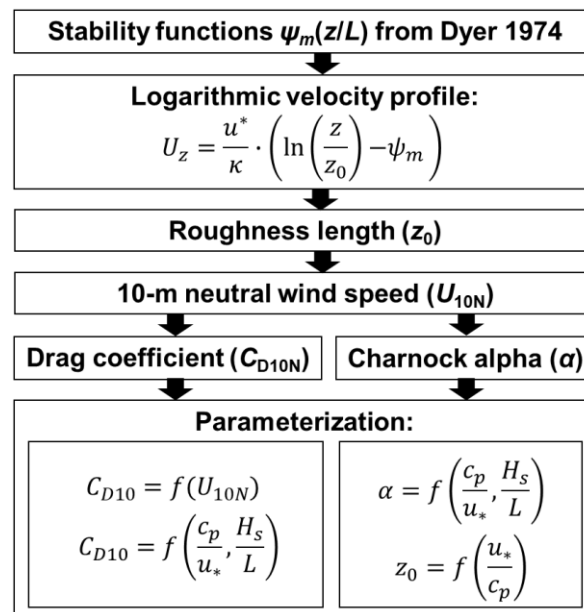
Fig. 5.1 Flux calculation workflow for the parameterization from the observation data

First, the drag coefficient relations were set up, both as a function of wind speed and wave parameters, like wave age. After that Charnock-alpha values and one average Charnock constant were calculated for the whole merged timeseries. Charnock-alpha, and other parameters like the roughness length were analyzed if there is any relationship between them and the wave parameters, wave age and wave steepness.

The momentum and heat flux estimations have been done with the iterative Monin-Obukhov similarity theory (MOST) and atmospheric stability functions. The calculation starts with initial guesses of the stability functions ($\psi_m = \psi_m = \psi_m = 0$), roughness length ($z_0 = z_{0H} = z_{0q} = 0.001$ m) and the Obukhov length (L = 10). Then the iteration starts with the calculation of the friction velocity, temperature scale and the scale of mixing ratio using Eq. 2.16,Eq. 2.17 and Eq. 2.18. Then the Obukhov length can be calculated from Eq. 2.15, and z/L can be calculated. Then the stability functions can be calculated from z/L using Eq. 2.19 and Eq. 2.23 for momentum, Eq. 2.20 and Eq. 2.24 for heat fluxes. After that the roughness lengths are calculated either from set up functions or constants using the already calculated friction velocity. Until the Obukhov length is not close enough to the lastly calculated or initially guessed one or the iteration reaches its preset maximum number value, the calculation continues. When it is finished, sensible and latent heat are calculated from the temperature scale and the scale of mixing ratio.

Results will be the estimated values of:

u_*	[m/s]	momentum flux
HT_s	[W/m^2]	sensible heat flux
L_vE	[W/m^2]	latent heat flux

5.2   Wave data processing & calculation

The acoustic surface tracking data from the Nortek Signature instrument were post-processed to get the wave parameters. The instrument took 4096 samples at 4 Hz for every 20-minute-long burst, so one burst measurement was 17.07-minute-long and then there was 2.93 minutes pause. The processing was done using own MATLAB scripts which consisted of 20-minute-average calculation, spike filtering with linear interpolation, detrending and deriving bulk parameters with spectral analysis following Holthujsen (2007). A typical wave spectrum can be seen in Fig. 5.2. The significant wave height was calculated from the first-order moment (m_0) of the wave spectrum:

$$H_s = H_{m0} = 4\sqrt{m_0}$$

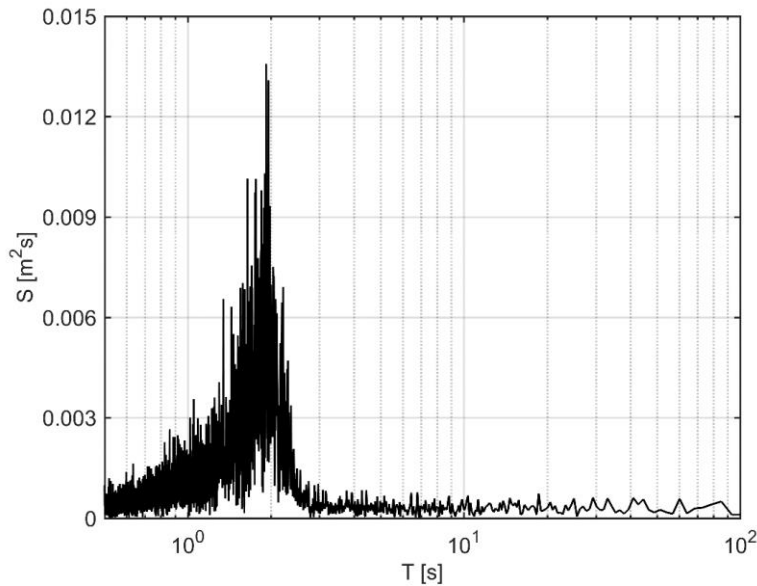<div align="right">Eq. 5.1</div>

Fig. 5.2 Typical wave spectrum for one burst measurement

The zero-crossing method was also used as a control, but there was very low deviation between the results of the two methods.

The post-processed measured wave data were the following:

H_s	[m]	significant wave height
f_p	[1/s]	peak frequency of the spectrum
T_p	[s]	wave period corresponding to the peak frequency
k	[-]	wavenumber
L	[m]	wavelength
H_s/L	[-]	wave steepness
c_p	[m/s]	wave phase velocity
c_p/u_*	[-]	wave age (u_* from atmospheric data)
u_*/c_p	[-]	inverse wave age

For those stations (like A and C) or for time periods at station B without wave measurements, wave parameters were estimated using the US Army Corps' Shore Protection Manual (SPM). The method was applied to MATLAB. The significant wave height and the average wave period was estimated from the wind speed, water depth and the fetch. The fetch was calculated from the coordinates of the station, the wind direction and coordinates of the shoreline of the lake.

The wave data has been filtered with QA & QC filters as the wind data, which consisted of a restriction of the analysis to fetch-limited conditions and so filtering out duration-limited conditions and also a minimum limiter of $H_s > 5$ cm has been applied because the use of wave formulation based estimations.

6   Results

In this chapter, the results of the data processing, momentum and heat flux observations and estimations are presented in detail.

First, a two-day-long timeseries of wind speed, wind direction and wave height can be seen in Fig. 6.1 a-b. In Fig. 6.1c the σ_w/u_* is shown, which characterizes the turbulence and the atmospheric stability. The stratification is neutral when it equals 1.25. The d, e, f panels of Fig. 6.1 show the measured momentum, sensible and latent heat flux values. The solid line shows the raw data and the red circles are the filtered data from the QA and QC filters detailed in the previous chapter.

Later in this chapter, the results of the momentum and heat flux estimations will be shown. First, with bulk parameterization using the drag and heat transfer coefficients, then the results of the necessary roughness length calculations will be shown for the estimation with MO method, and the results of the estimation itself will follow those. Last, the simple linear flux estimations are shown, which does not apply the MOST and the stability functions, unlike any other method which are shown in the study.
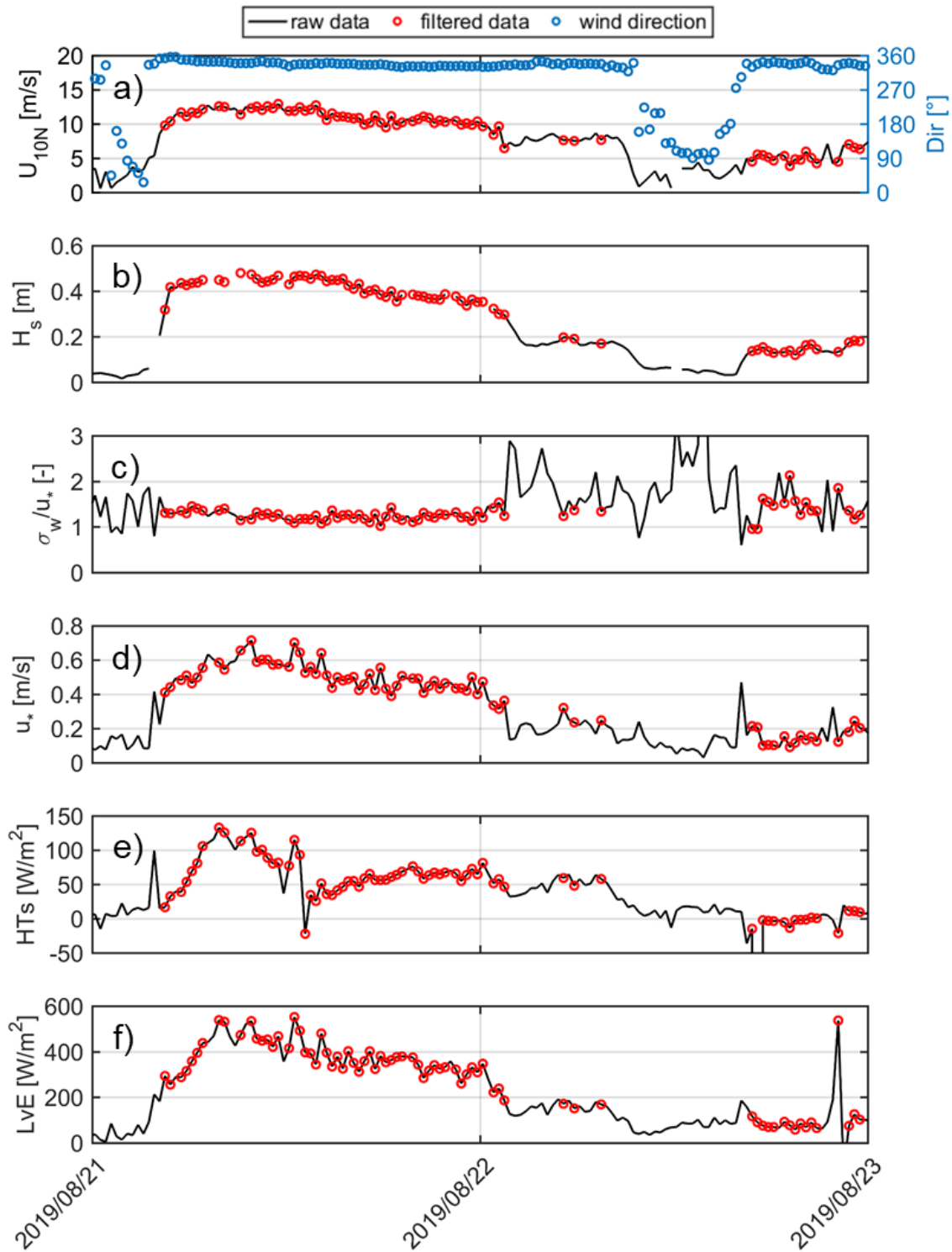
Fig. 6.1 Timeseries of wind speed (a), wave height (b), turbulence characteristics (c), momentum flux (d), sensible (e) and latent heat flux (f)

6.1   Drag and heat transfer coefficients

In this chapter the drag and heat coefficients are calculated for the bulk estimation of momentum and heat fluxes. The drag coefficient relations were derived both as a function of the 10-meter neutral wind speed and wave age.
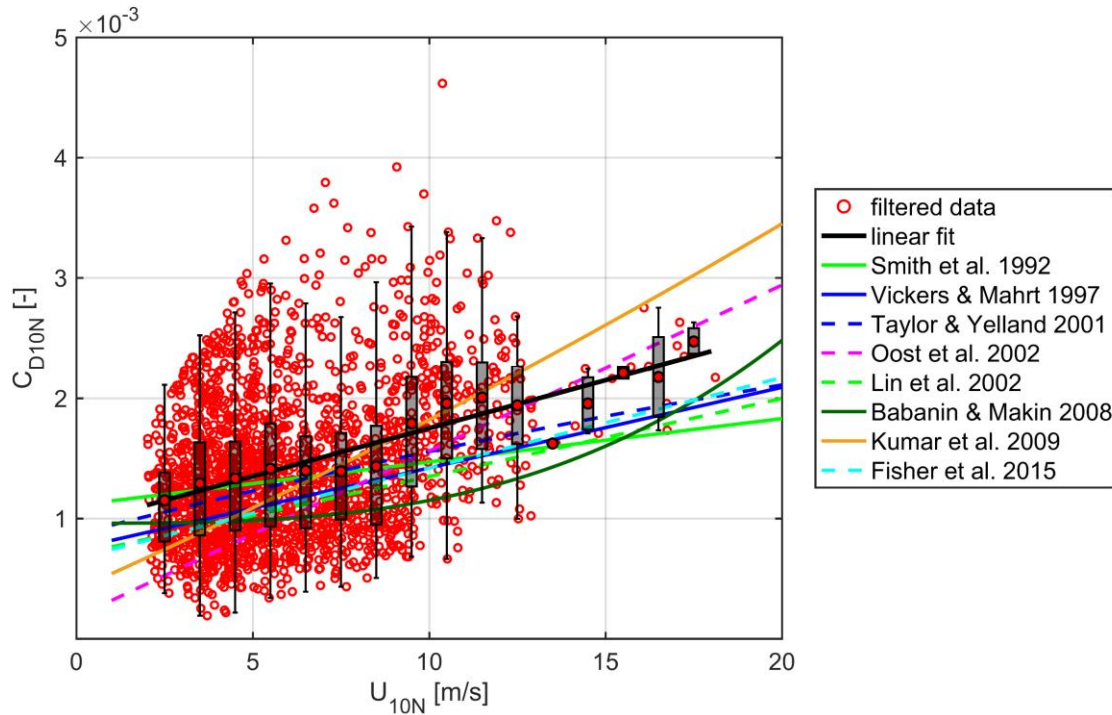
Fig. 6.2 10-m neutral drag coefficient as a function of wind speed

$$C_{D10N} = (0.95 + 0.08 \cdot U_{10N}) \cdot 10^{-3}$$

Eq. 6.1

The established equations (Eq. 6.1 and Eq. *6.2*) can be seen in Fig. 6.2 and Fig. 6.3, and they noticeably differ from ones in the literature. The literature functions of drag coefficient as a function of wind speed are below the results and they are less steep. These functions would underestimate the momentum exchange. The linear equation from Oost et al. (2002) would well estimate the momentum flux for winds above 8 - 9 m/s, but it is too steep and it would not be accurate for lower winds, but they had 9 km of fetch, which is about three-times higher than ours at Lake Balaton. Vickers and Mahrt (1997) have similar fetch of 2 - 5 km as in our case. The slope of their linear is almost the same as for us, but their drag coefficients are steadily lower. The drag coefficient - wave age relation of the results differs even more remarkably to the literature functions, but they would overestimate the momentum flux. These figures ensure the hypothesis: for the fetch limited young waves new relations had to be formulated.
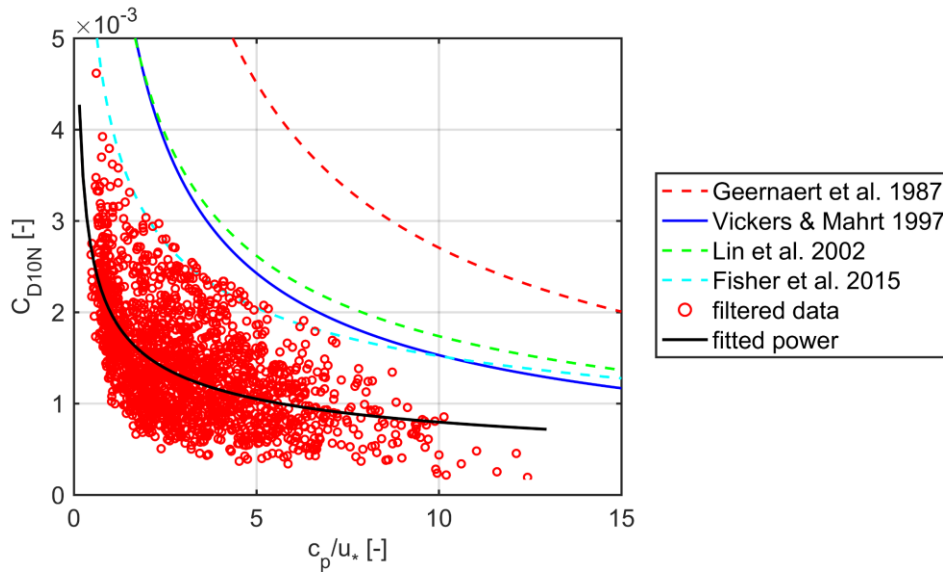
Fig. 6.3 10-m neutral drag coefficient as a function of wave age

$$C_{D10N} = 0.002 \cdot \left(\frac{c_p}{u_*}\right)^{-0.4}$$

Eq. 6.2

The sensible and latent heat transfer coefficients can be seen in Fig. 6.4 and Fig. 6.5 as a function of wind speed multiplied with heat and humidity differences. They both show high uncertainty which decreases with higher wind speed. Constant values were chosen for the coefficients, $C_{H10N} = 0.00135$ and $C_{q10N} = 0.001$, which was the best fit to the high wind speeds or the differences in heat and humidity.
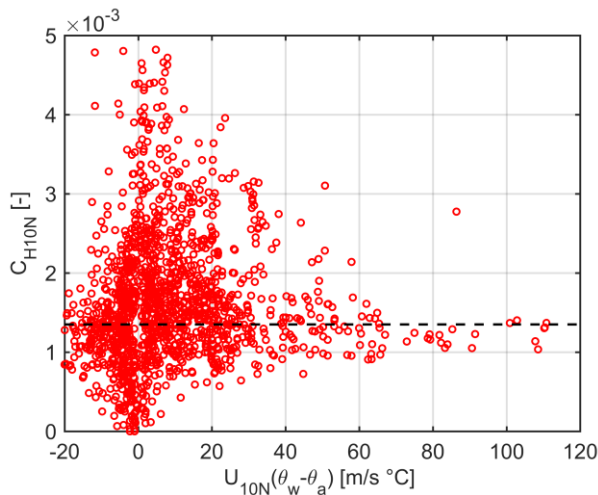
Fig. 6.4 10-m neutral sensible heat transfer coefficient as a function of wind speed multiplied with potential temperature difference
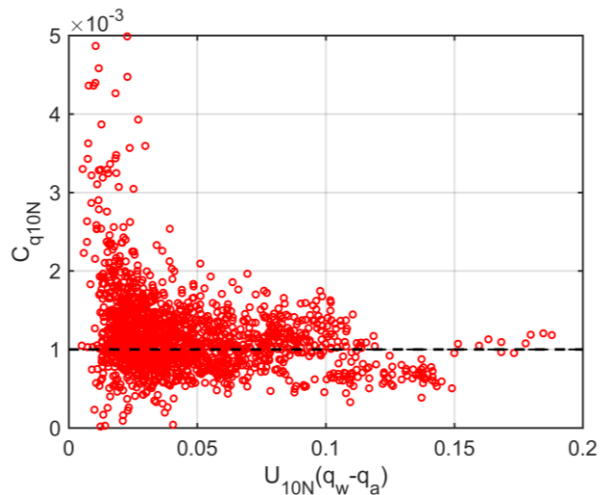
Fig. 6.5 10-m neutral latent heat transfer coefficient as a function of wind speed multiplied with specific humidity difference

6.2   Roughness length of momentum

6.2.1 Charnock constant

The empirical probability density function (PDF) of the logarithmic alpha values can be seen in Fig. 6.6. The mean of the histogram provides the value of $\alpha = 0.035$, which is about three-times higher than the literature average, $\alpha = 0.012$, but it is less then $\alpha = 0.073$ measured with RASEX (Vickers and Mahrt 1997). With calculated constant value of the Charnock-α, the roughness length can be calculated from Eq. 2.32 for the estimation of fluxes with the MO method.
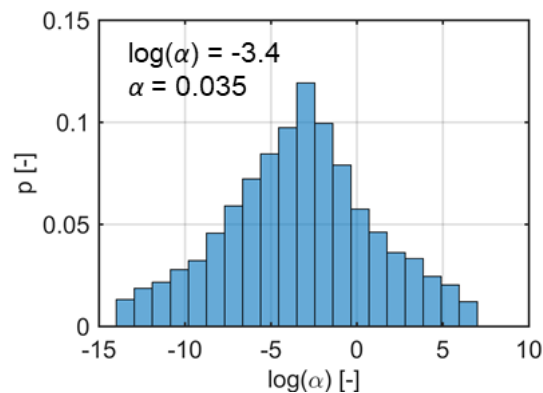
Fig. 6.6 PDF of logarithmic Charnock-alpha values

6.2.2 Wave age

A Charnock-type relation was searched to incorporate the effect of the wave field, as there are many formulations in the literature for that. But as it can be seen in Fig. 6.7, very weak relation was found between Charnock alpha and wave age, and also the measured data points are quite far from the literature functions. While alpha cannot be, but the surface roughness can be directly related to the wave age (Fig. 6.8). An advantage of this equation (Eq. 6.1) is that it avoids self-correlation when both Charnock alpha and roughness length are function of the friction velocity.
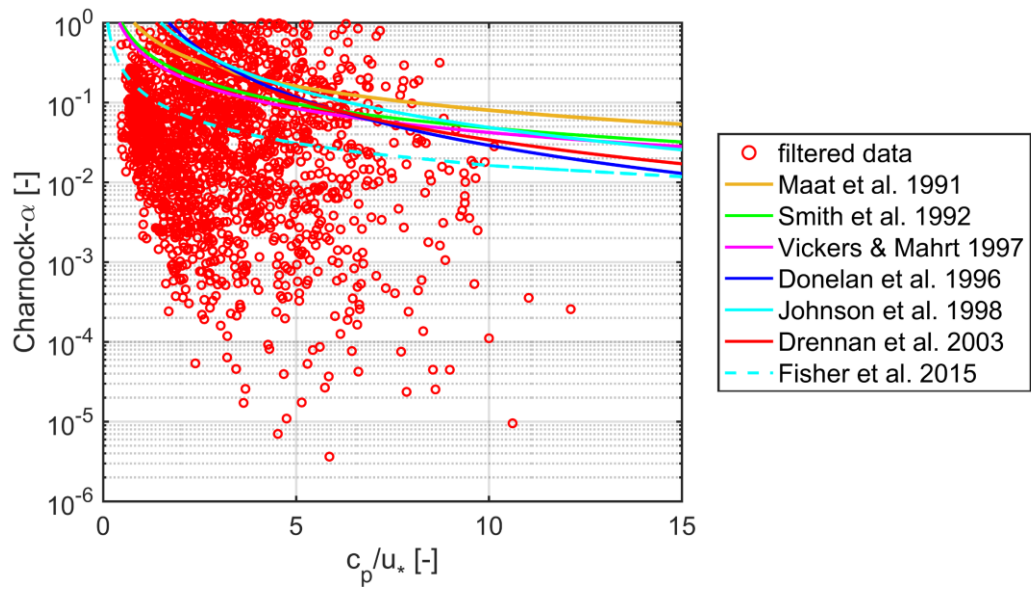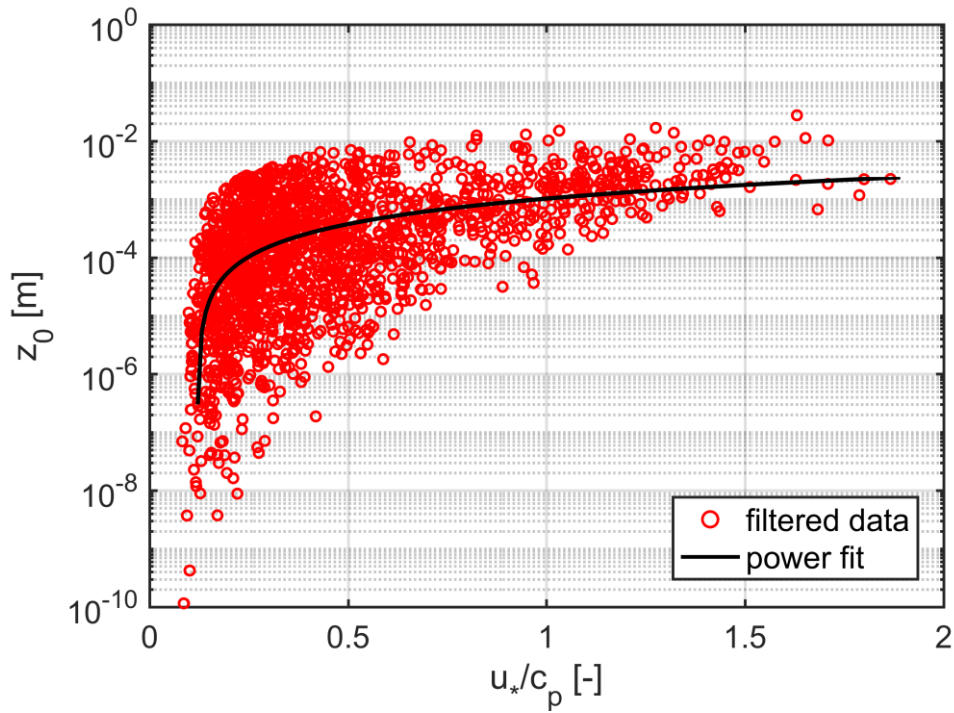
Fig. 6.7 Charnock-α as a function of wave age

Fig. 6.8 Roughness length as a function of inverse wave age

$$z_0 = 0.0012 \cdot \left(\frac{u_*}{c_p} - 0.12 \right)^{1.2}$$

Eq. 6.1

6.2.3 Wave steepness

Wave steepness also can represent the effect of the waves field to the roughness length of momentum as it was showed in some of the literature. In Fig. 6.9 the wave steepness can be seen as a function of wind speed. It shows that under 5 m/s wind speed, the steepness is very uncertain and also that after reaching a steepness of ~0.05, the waves break, and it means that white-capping or wave breaking occurs. Looking at the roughness length as a function of wave steepness in Fig. 6.10, it can be stated that there is no relation between them. As the wave steepness cannot be related to the roughness, it cannot be used for flux estimation with the MO method either.
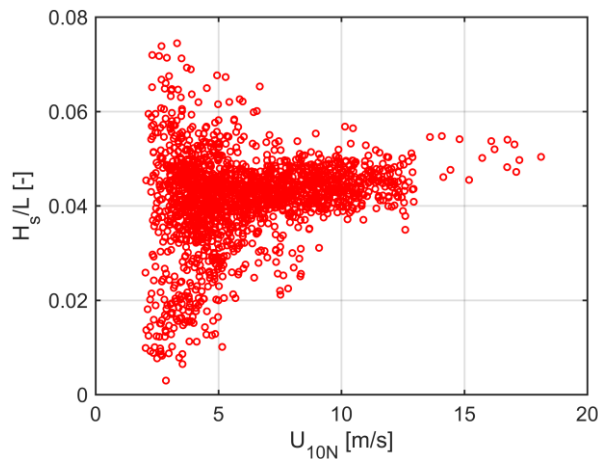
Fig. 6.9 Wave steepness as
a function of wind speed
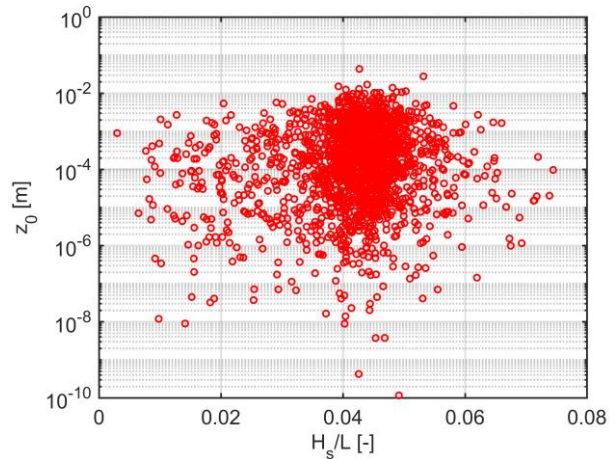
Fig. 6.10 Roughness length as
a function of wave steepness

6.3   Roughness lengths of heat and humidity

Similarly, like previously with the roughness length for momentum, relations were searched between the roughness lengths of heat and humidity and the wave parameters for the estimation with the MO method. As it can be seen in Fig. 6.11 with the example of roughness length of sensible heat (z_{0H}), there are very weak relationships in the case of friction velocity, inverse wave age and wave steepness as well. The results are the same for the roughness length of humidity.
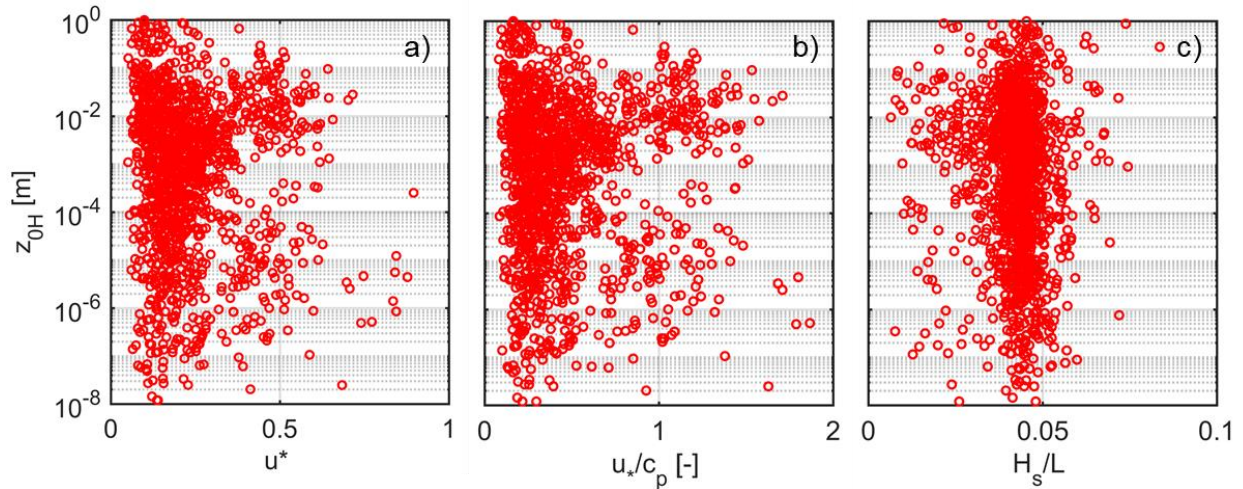
Fig. 6.11 Roughness length of sensible heat as a function of friction velocity (a),
inverse wave age (b) and wave steepness (c)

Therefore, the roughness lengths of heat and humidity were chosen to be characterized with constant values. The means of the histograms (Fig. 6.12Fig. 6.13) provide the values of $z_{0H} = 10^{-3}$ and $z_{0q} = 5 \cdot 10^{-7}$. The MO estimations of heat fluxes have been done using these calculated constants.
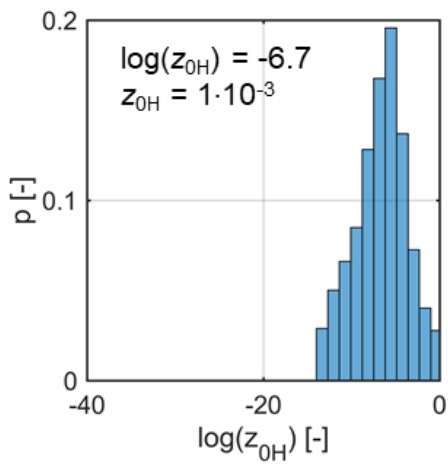

Fig. 6.12 PDF of logarithmic values
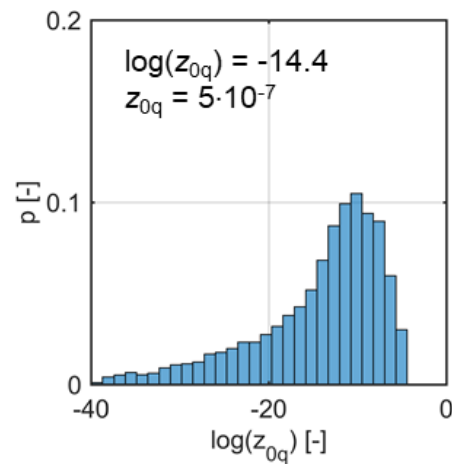*of roughness length of heat*

Fig. 6.13 PDF of logarithmic values of
roughness length of specific humidity

6.4   Estimation of fluxes

6.4.1 Monin-Obukhov (MO)

The iterative momentum and heat flux estimation is based on the Monin-Obukhov similarity theory (MOST). The calculation was done by using the slow measurements for the same 20-minute-averages and applying the atmospheric stability functions and the calculated Charnock constant and the wave age relation for the roughness length of momentum and the constant roughness lengths of heat and humidity.

In Fig. 6.14 a-c, the results of the measured and estimated momentum, sensible and latent heat flux values are shown with the Charnock constant. The correlation coefficient (R^2) has the highest value of 0.88 for the momentum flux and it has lower values for the heat fluxes. In Fig. 6.14 d-f, the results of the other flux estimation method are shown which consider the effect of the wave field in the roughness length of momentum. Here, the measured wave parameters were used for the roughness length estimation. The results barely differ from the ones obtained with the Charnock constant, and the correlation coefficients are a little lower than that too. Consequently, the momentum and heat flux estimation does not get any more accurate with the MO method as it was expected using the measured wave data.

However, altogether the MO method performs well. Due to observational uncertainties in the EC data, the correlation coefficients of 0.88 and 0.86 for the momentum flux estimation probably could not get any higher than those. In the case of sensible heat flux, the lower values seem more accurate than it was with momentum flux, but at the high values, the scatter opens and some of the fluxes are very much overestimated, and some of them are underestimated. The latent heat fluxes are also quite accurately estimated for lower values, but they are overestimated for the high ones.
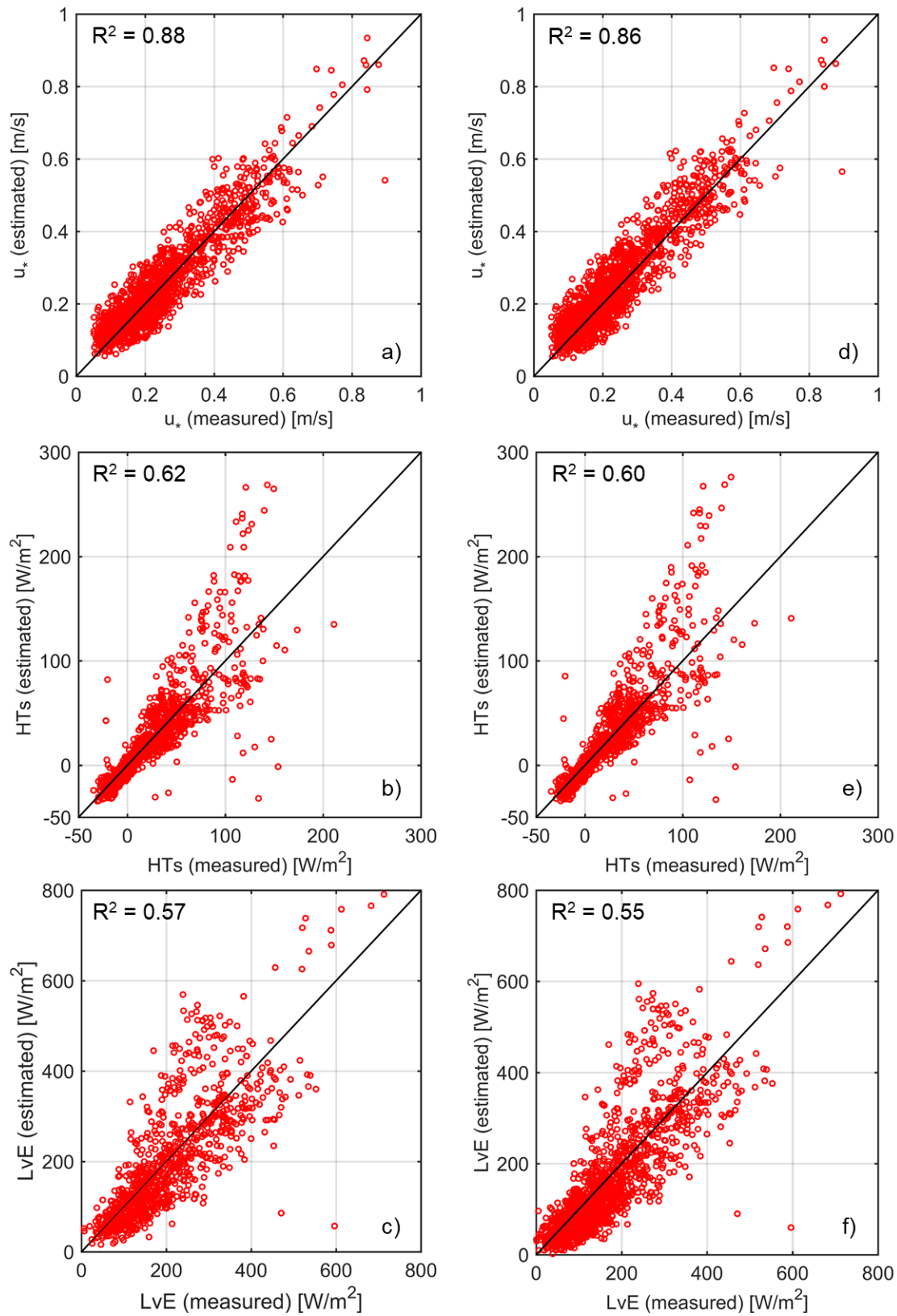
Fig. 6.14 Results of the flux estimation with Charnock constant (a-c) and wave age relation (d-f)

6.4.2 Linear regression

Recently, there are examples in the literature about using linear equations for momentum fluxes (Andreas et al. 2012; Vickers et al. 2015). The linear regression (Eq. 6.3) between the friction velocity and the wind speed is quite strong, with $R^2 = 0.85$ (Fig. 6.15). This relation is not based on the MOST and the stability functions, but it does make the momentum flux estimation more simple and faster and this is probably the most cost-efficient method of all which were shown in this study earlier. Simple estimation could have been done using the wind speed measured at ~ 6 m, which had just as strong relationship with the momentum flux, but this way, the method is more unified for measurements at different heights and comparison as well.
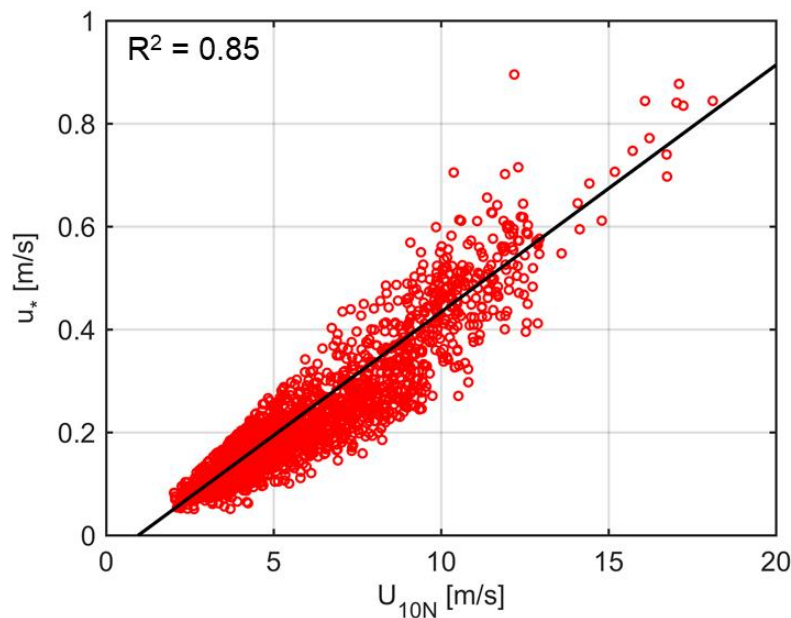

Fig. 6.15 Momentum flux as a function of wind speed

$$u_* = 0.048 \cdot U_{10N} - 0.046$$

Eq. 6.3

In the case of heat fluxes the linear estimations are better than other methods showed previously, which all are based on the MOST. The correlation coefficient of the linear relation for the sensible heat flux shows strong relationship (Fig. 6.16 andEq. 6.4).
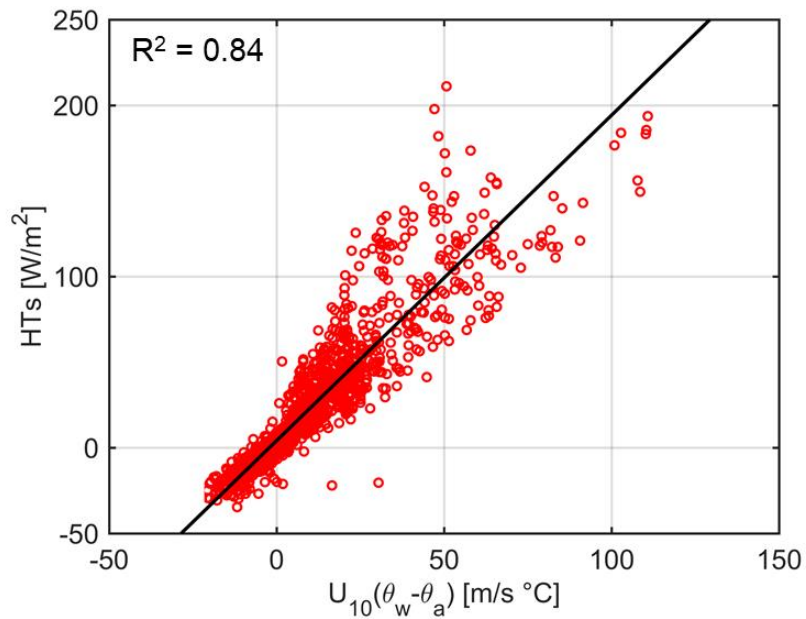
*Fig. 6.16 Sensible heat flux as a function of wind speed
multiplied with potential temperature difference*

$$HTs = 1.9 \cdot U_{10N} \cdot (\theta_w - \theta_a) + 4.2$$
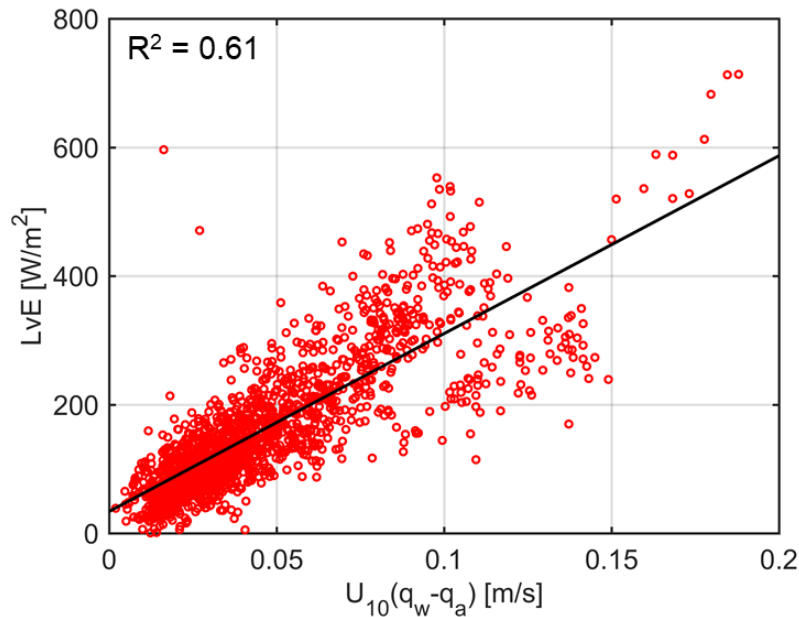
Eq. 6.4

*Fig. 6.17 Latent heat flux as a function of wind speed
multiplied with specific humidity difference*

$$L_v E = 2765 \cdot U_{10N} \cdot (q_w - q_a) + 34$$

Eq. 6.5

7   Discussion

The accuracy of momentum and heat flux estimation methods are compared using correlation coefficients. They were calculated for all estimated fluxes and their measured values (Table 7.1). Altogether, the momentum flux estimations are the most robust of any methods, with strong R^2 values between 0.84 and 0.90. The heat fluxes somewhat stay behind, but correlation coefficients are between 0.55 and 0.66, which are moderate values. Very interesting to see that the simplest linear relations perform the best if all turbulent flux analysis are counted together.

Table 7.1 Correlation coefficients of estimated momentum and heat fluxes for different methods

	Bulk		Monin-Obukhov		Linear regression
	C_D (U) C_H, C_q = const.	C_D (c_p/u_*)	z_0 (Charnock α), z_{0H}, z_{0q} = const.	z_0 (u_*/c_p), z_{0H}, z_{0q} = const.	
u_*	0.86	0.90	0.88	0.86	0.84
HTs	0.58	-	0.62	0.60	0.84
LvE	0.66	-	0.57	0.55	0.63

7.1   Spatial variability

In Fig. 7.1 a 20-hour-long wind event was analyzed by means of stations B and C to explore the spatial variability of the wind and momentum exchange. The two upper panels of Fig. 7.1 show the measured time series of wind speed and wind direction. The wind direction was the prevailing N-NW direction in both stations. According the internal boundary layer (IBL) development theory it is expected that the wind speed would be higher in station C where the fetch is 6 km compared to B where it is only 3.5 km. But instead of that, the wind speed is quite similar, but slightly smaller at the station with longer fetch, which means some other meso-scale processes dominated the wind field above the lake.

Wave parameters have been estimated for station C from the local wind speed and fetch, since there were no wave measurements there. In one hand, the measured and estimated wave heights (Fig. 7.1c) are quite similar at the two locations, in the other hand the wave age (Fig. 7.1d) is remarkably higher at station C with the longer fetch. In Fig. 7.1e you can see the measured friction velocity values from which the Charnock constants were derived for the grey-colored time period. It is α = 0.020 for station C with the longer fetch and α = 0.046 for offshore station B in the middle of the lake. So, the spatial variability is quite high, and the momentum flux cannot be estimated with one constant alpha value for the whole bay. However, this spatial variation can be captured in the wave field, that can be accurately estimated using the local wind measurement if there are no wave measurements available.
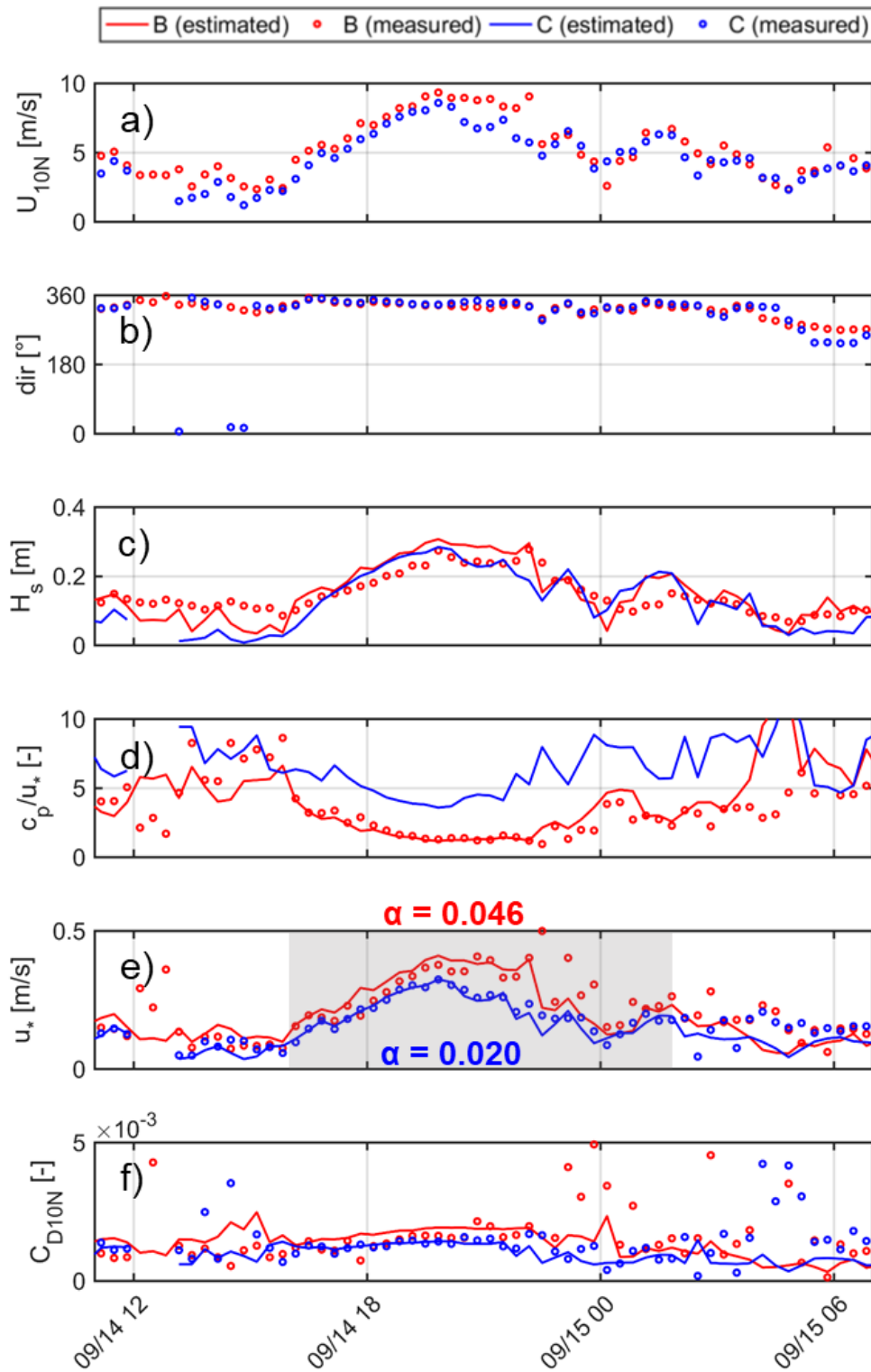
Fig. 7.1 Wind speed (a), wind direction (b), significant wave height (c), wave age (d), momentum flux (e) and drag coefficient (f) time series of a 20-hour-long wind event

Consequently, the wave age relation-based roughness length estimation can capture the spatial variation of the momentum exchange. Applying the earlier derived roughness length equation as a function of wave age, the estimated momentum fluxes agree well with the measured values on both stations (Fig. 7.1e). In terms of drag coefficients, smaller deviation has been observed, but still the drag coefficient is continuously smaller at the station with higher fetch (Fig. 7.1f). It was stated in the past chapter that both Charnock constant and wave age based MO estimation methods are equally good, but the analysis of the two stations resulted that the wave age shows more accurately the spatial variability of momentum flux.

7.2   Uncertainties

Despite the accuracy of the momentum flux estimation with various methods showed earlier, there are many sources of uncertainties that need to be considered. 75 % percent of data were filtered out to establish the relations to ensure the accuracy of the estimation. These quality assurance filters have been applied: $\Delta U_{10N} < 50$ %, $\Delta dir <$ 30 °, $U_{10N} > 2$ m/s, $u_* > 5$ cm/s, $H_s > 5$ cm. These minimum limiters needed to be applied to ensure the stationarity, to filter out uncertainly measured low winds with small waves for the estimation as well, because of the derived wave formulations. In Fig. 7.2 and Fig. 7.3 the raw data are shown with grey color and the filtered data with red color together. 90 % of the filtered-out data are very low winds, under 3-4 m/s or so. Free-convection (Abdella and D'Alessio 2005), or lake-breeze events (Metzger et al. 2018) might be responsible processes and new separate formulas must be developed in the future to extend the estimation for low winds. To my knowledge this type of research was only performed in oceanographic circumstances (Edson et al. 2007).
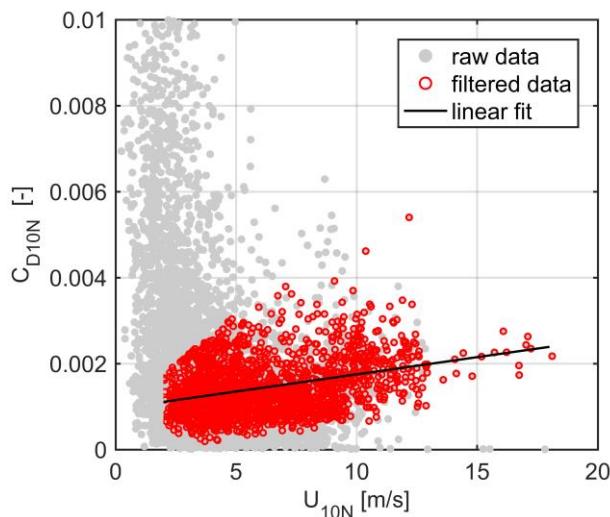

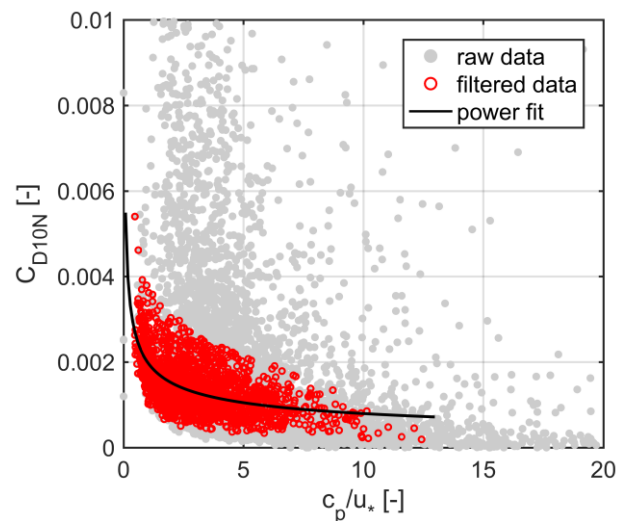*Fig. 7.2 Drag coefficient as a function of 10-m wind speed (raw and filtered data)*

Fig. 7.3 Drag coefficient as a function of wave age (raw and filtered data)

7.3   Effect of stratification

The applied stability functions also have uncertainty, because they were derived for different, mostly for oceanographic environment as well, and so far, all the other formulations could not be applied and needed to be newly derived for shallow lakes. Fig. 7.4 shows the z/L stability conditions as a function of drag coefficient, temperature difference and wind speed. z/L has a dependence of all three, but the most visible is with the drag coefficient. New stability functions could be set up using this relation if necessary.
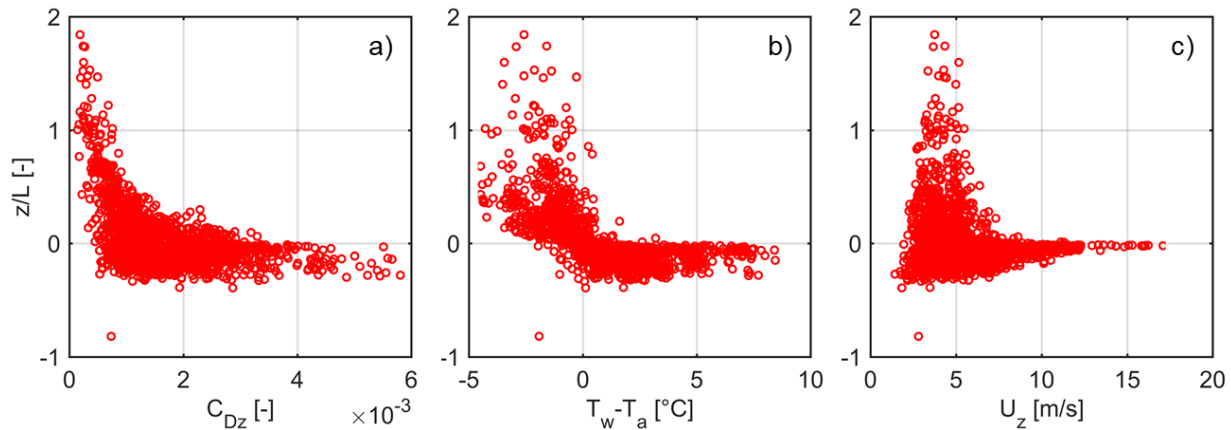

Fig. 7.4 Stability conditions as a function of drag coefficient (a),
temperature difference (b) and wind speed (c)

In order to analyze the effect of the stratification to the results, the estimation with MO method was repeated with all stability functions set zero ($\psi_m = \psi_H = \psi_q = 0$) and it can be seen in Fig. 7.5 the analysis showed very low effect of atmospheric stability and so the correction of stability functions are not necessary. This also strengthen the usage of simple linear functions instead of iterative algorithms.
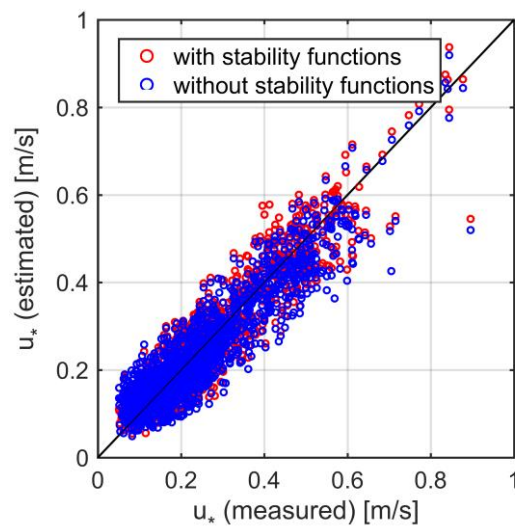

Fig. 7.5 MO estimation of momentum flux with and without stability functions

8   Summary and conclusions

To summarize and conclude this study, the bulk estimation works robust with five kinds of methods which were analyzed, with the drag and heat coefficients both as a function of wind speed and wave age, the MOST based estimation with roughness lengths both with the Charnock constant and as a function of wave age as well as with very simple linear regression with wind speed and temperature and humidity differences. The hypothesis was proven, that all new relations had to be established for this strongly fetch limited environment, that is highly influenced by breaking and white-capping waves and the generally high surface roughness characterization of the water surface in shallow lakes. The calculated Charnock constant, $\alpha = 0.035$ is three-times higher than the literature average, $\alpha = 0.012$, except for RASEX, $\alpha = 0.073$ (Vickers and Mahrt 1997). The roughness length - inverse wave age relationship has been established, which avoids self-correlation, unlike when using the Charnock alpha for roughness length estimation. This wave age based estimation method can take into account the spatial variability of the momentum flux and is suggested to use if several wind observations are available and it can be used for analysis of IBL development. Despite the strong relationships for momentum flux and moderate ones for heat fluxes established, they are only valid if strictly filtered data are used. 80% of the raw data were filtered out following literature of quality control for eddy-covariance data. The estimation has generally high uncertainty at low winds. Applying the linear regression has many advantages, because is not based on the MOST and the stability functions which can be uncertain, but it does make the momentum flux estimation more simple and faster method of all shown in this study.

9   Outlook

In the future new formulas should be developed to extend the estimation of turbulent fluxes for the buoyancy dominated low winds.

The dynamics of surface waves and the turbulent mixing in the waterside surface boundary layer (SBL) should be analyzed comprehensively. The given detailed analysis in this study on momentum and heat fluxes of the airside will be followed with the quantification of the turbulent mixing of the waterside in the future. The mixing can be analyzed with the dissipation of turbulent kinetic energy (TKE) from high frequency current meter and current profile measurement data available from the ADV, Signature and Aquadopp instruments for the analyzed station in Lake Balaton.

The energy budget of the lake could be closed using the heat fluxes. The EC technique cannot measure large-scale eddies in the atmosphere, only small-scale turbulent fluctuations, which means the sensible heat is probably larger than what the Bowen-ratio results. This question can be properly analyzed with measured datasets.

Finally, these new formulas established in this study can provide accurate boundary conditions for a hydrodynamic model, which could serve as a base of a lake forecasting system in the future if the model is detailed enough both in the description of the physical processes and in spatial resolution.

10   Acknowledgement

I would like to express my special thanks of gratitude to:

- Péter Torma for leading my work in the past year in general. He was very helpful at the calculations and tricks in MATLAB, at trying to give explanations and solutions for any problems that came up and for showing me how to make a little more sophisticated publications.
- Tamás Weidinger from the Department of Meteorology at ELTE for initiating the FIMO-CROHUN project and continuous cooperation in measurements.
- everyone from the Department of Hydraulic and Water Resources Engineering at BME who helped and made possible the measurements, especially András Rehák for regularly climbing the six-meter-tall stations and diving underwater to make sure all instruments work fine.

11 References

Abdella, K. and S. J. D. D'Alessio. 2005. "On the Parameterization of the Roughness Length for the Air-Sea Interface in Free Convection." *Environmental Fluid Mechanics* 4(4):451–53.

Andreas, Edgar L., Larry Mahrt, and Dean Vickers. 2012. "A New Drag Relation for Aerodynamically Rough Flow over the Ocean." *Journal of the Atmospheric Sciences* 69(8):2520–37.

Babanin, Alexander V. and Vladimir K. Makin. 2008. "Effects of Wind Trend and Gustiness on the Sea Drag: Lake George Study." *Journal of Geophysical Research* 113(C2):C02015.

Brutsaert. 1982. *Evaporation into the Atmosphere*. D. Reidel Publishing Company.

Charnock, H. 1955. "Wind Stress on Water: An Hypothesis." *Quarterly Journal of the Royal Meteorological Society* 81(349):320–32.

Donelan, Mark A., Fred W. Dobson, Stuart D. Smith, and Robert J. Anderson. 1993. "DonelanOntheDependenceSeaSurfRoughOnWaveDevelopment93.Pdf." *Journal of Physical Oceanography* 23:2143–49.

Drennan, William M., Hans C. Graber, Daniele Hauser, and Céline Quentin. 2003. "On the Wave Age Dependence of Wind Stress over Pure Wind Seas." *Journal of Geophysical Research* 108(C3):8062.

Dyer, A. J. 1974. *A Review of Flux-Profile Relationships*. Boundary-Layer Meteorology Vol. 7.

Edson, B. Y. James, T. Crawford, J. Crescenti, T. Farrar, N. Frew, G. Gerbi, C. Helmis, T Hristov, D. Khelif, A. Jessup, M. Li, L. Mahrt, W. Mcgillis, A. Plueddemann, L. Shen, E. Skyllingstad, T. Stanton, P. Sullivan, J. Sun, J. Trowbridge, D. Vickers, C. Zappa. 2007. "Layers and Air-Sea Transfer." American Meteorological Society..

Edson, James B., Venkata Jampana, Robert A. Weller, Sebastien P. Bigorre, Albert J. Plueddemann, Christopher W. Fairall, Scott D. Miller, Larry Mahrt, Dean Vickers, and Hans Hersbach. 2013. "On the Exchange of Momentum over the Open Ocean." *Journal of Physical Oceanography* 43(8):1589–1610.

Fairall, C. W., E. F. Bradley, J. E. Hare, A. A. Grachev, and J. B. Edson. 2003. "Bulk Parameterization of Air-Sea Fluxes: Updates and Verification for the COARE Algorithm." *Journal of Climate* 16(4):571–91.

Fisher, Alexander W., Lawrence P. Sanford, and Steven E. Suttles. 2015. "Wind Stress Dynamics in Chesapeake Bay: Spatiotemporal Variability and Wave Dependence in a Fetch-Limited Environment*." *Journal of Physical Oceanography* 45(10):2679–96.

Foken, Thomas, Mathias Gockede, Matthias Mauder, Larry Mahrt, Brian Amiro, and William Munger. 2004. *Handbook of Micrometeorology: A Guide for Surface Flux Measurement and Analysis: Chapter 9: POST-FIELD DATA QUALITY CONTROL*.

Foken, Thomas. 2008. "Micrometeorolgy". Springer Science & Business Media

Geernaert, G. L., S. E. Larsen, and F. Hansen. 1987. "Measurements of the Wind Stress, Heat Flux, and Turbulence Intensity during Storm Conditions over the North Sea." *Journal of Geophysical Research* 92(C12):13127.

Holthujsen, L. H. 2007. *Waves in Oceanic and Coastal Waters*. Cambridge University Press.

Johnson, H. K., J. Højstrup, H. J. Vested, and S. E. Larsen. 1998. "On the Dependence of Sea Surface Roughness on Wind Waves." *Journal of Physical Oceanography* 28(9):1702–16.

Li, Zhaoguo, Shihua Lyu, Lin Zhao, Lijuan Wen, Yinhuan Ao, and Shaoying Wang. 2016. "Turbulent Transfer Coefficient and Roughness Length in a High-Altitude Lake, Tibetan Plateau." *Theoretical and Applied Climatology* 124(3–4):723–35.

Lin, Weiqi, Lawrence P. Sanford, Steven E. Suttles, and Richard Valigura. 2002. "Drag Coefficients with Fetch-Limited Wind Waves." *Journal of Physical Oceanography* 32(11):3058–74.

Maat, N., C. Kraan, and W. A. Oost. 1991. "The Roughness of Wind Waves." *Boundary-Layer Meteorology* 54(1–2):89–103.

Mauder, Matthias and Thomas Foken. 2011. "Documentation and Instruction Manual of the Eddy-Covariance Software Package TK3." *Arbeitsergebnisse* 3(46):60, ISSN 1614-8916.

Metzger, Jutta, Manuela Nied, Ulrich Corsmeier, Jörg Kleffmann, and Christoph Kottmeier. 2018. "Dead Sea Evaporation by Eddy Covariance Measurements vs. Aerodynamic, Energy Budget, Priestley-Taylor, and Penman Estimates." *Hydrology and Earth System Sciences* 22(2):1135–55.

Monin, A. S. and A. M. Obukhov. 1954. "Basic Laws of Turbulent Mixing in the Atmosphere near the Ground." *Tr. Akad. Nauk SSSR Geofiz. Inst* 24(151):163–87.

Oost, W. A., G. J. Komen, C. M. J. Jacobs, and C. Van Oort. 2002. "New Evidence for a Relation between Wind Stress and Wave Age from Measurements during ASGAMAGE." *Boundary-Layer Meteorology* 103(3):409–38.

Rajesh Kumar, R., B. Prasad Kumar, A. N. V. Satyanarayana, D. Bala Subrahamanyam, A. D. Rao, and S. K. Dube. 2009. "Parameterization of Sea Surface Drag under Varying Sea State and Its Dependence on Wave Age." *Natural Hazards* 49(2):187–97.

Shabani, Behnam, Peter Nielsen, and Tom Baldock. 2014. "Direct Measurements of Wind Stress over the Surf Zone." *Journal of Geophysical Research: Oceans* 119(5):2949–73.

Smith, Stuart D., Robert J. Anderson, Wiebe a Oost, C. Kraan, Nico Maat, Janice DeCosmo, Kristina B. Katsaros, Kenneth L. Davidson, Karl Bumke, Lutz Hasse, and Helen M. Chadwick. 1992. "Wind Stress and Drag Coefficients :" *Boundary-Layer Meteorology* 60:109–42.

Taylor, P. K. and M. J. Yelland. 2001. "The Dependence of Sea Surface Roughness on the Height and Steepness of the Waves." *Journal of Physical Oceanography* 31(2):572–90.

Torma, Péter. 2016. "Modelling Wind-Driven Shallow Lake Hydrodynamics and Thermal Structure." *Ph.D. Thesis.*

Vickers, Dean and Larry Mahrt. 1997. "Fetch Limited Drag Coefficients." *Boundary-Layer Meteorology* 85(1):53–79.

Vickers, Dean, Larry Mahrt, and Edgar L. Andreas. 2015. "Formulation of the Sea Surface Friction Velocity in Terms of the Mean Wind and Bulk Stability." *Journal of Applied Meteorology and Climatology* 54(3):691–703.

Wang, Binbin, Yaoming Ma, Xuelong Chen, Weiqiang Ma, Zhongbo Su, and Massimo Menenti. 2015. "Observation and Simulation of Lake-Air Heat and Water Transfer Processes in a High-Altitude Shallow Lake on the Tibetan Plateau." *Journal of Geophysical Research* 120(24):12,327-12,344.

Wang, Binbin, Yaoming Ma, Weiqiang Ma, and Zhongbo Su. 2017. "Physical Controls on Half-Hourly, Daily, and Monthly Turbulent Flux and Energy Budget over a High-Altitude Small Lake on the Tibetan Plateau." *Journal of Geophysical Research* 122(4):2289–2303.

Webb, E. K., G. I. Pearman, and R. Leuning. 1980. "Correction of Flux Measurements for Density Effects Due to Heat and Water Vapour Transfer." *Quarterly Journal of the Royal Meteorological Society* 106(447):85–100.

Wilczak, James M., Steven P. Oncley, and Steven A. Stage. 2001. "Sonic Anemometer Tilt Correction Algorithms." *Boundary-Layer Meteorology* 99(1):127–50.

Xiao, Wei, Shoudong Liu, Wei Wang, Dong Yang, Jiaping Xu, Chang Cao, Hanchao Li, and Xuhui Lee. 2013. "Transfer Coefficients of Momentum, Heat and Water Vapour in the Atmospheric Surface Layer of a Large Freshwater Lake." *Boundary-Layer Meteorology* 148(3):479–94.

Yusup, Yusri and Heping Liu. 2016. "Effects of Atmospheric Surface Layer Stability on Turbulent Fluxes of Heat and Water Vapor across the Water-Atmosphere Interface." *Journal of Hydrometeorology* 17(11):2835–51.